JOC The Journal of Organic Chemistry

Article

pubs.acs.org/joc

Effect of Extended Benzannelation Orientation on Bergman and Related Cyclizations of Isomeric Quinoxalenediynes

Stephanie A. Valenzuela, Alondra J. Cortés, Zakery J. E. Tippins, Morgan H. Daly, Terell E. Keel, Benjamin F. Gherman,* and John D. Spence*

Department of Chemistry, California State University, Sacramento, 6000 J Street, Sacramento, California 95819, United States

Supporting Information

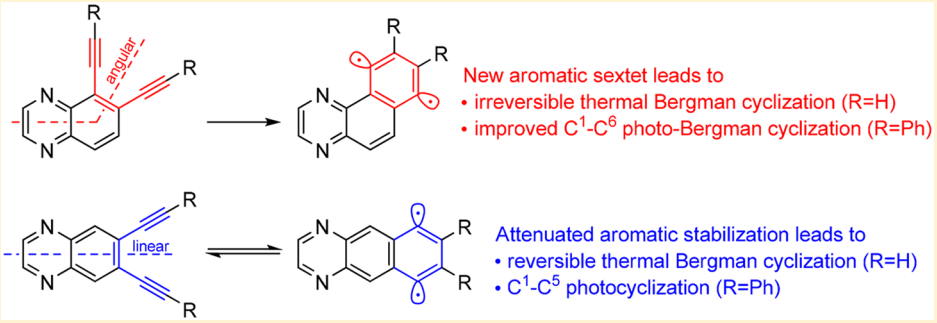

ABSTRACT: A combined computational and experimental study was conducted to examine the effect of extended benzannelation orientation on C^1-C^5 and C^1-C^6 cyclization of acyclic quinoxalenediynes. Calculations (mPW1PW91/cc-pVTZ//mPW1PW91/6-31G(d,p)) on terminal and phenylethynyl-substituted 5,6-diethynylquinoxaline and 6,7-diethynylquinoxaline showed C^1-C^6 Bergman cyclization as the favored thermodynamic reaction pathway, with larger C^1-C^6 preference for the angular quinoxalenediynes due to gain of a new aromatic sextet. Kinetic studies, as a function of 1,4-cyclohexadiene concentration, revealed retro-Bergman ring opening predominates over hydrogen atom abstraction ($k_{-1} > k_2$) for 6,7-diethynylquinoxaline while 5,6-diethynylquinoxaline undergoes irreversible Bergman cyclization indicative of a large retro-Bergman ring opening barrier ($k_2 > k_{-1}$). The effect of extended linear versus angular benzannelation on reaction pathway shows in the contrasting photocyclizations of phenylethynyl derivatives. While angular 5,6-diethynylquinoxalines gave exclusive C^1-C^6 photocyclization, linear 6,7-diethynylquinoxaline afforded C^1-C^5 fulvene products. Computed singlet−triplet gaps and biradical stabilization energies indicated weak interaction between the nitrogen lone pair and proximal radical center in angular 5,6-diethynylquinoxalines. The overall data indicates extended angular benzannelation effectively renders Bergman cyclization irreversible due to favorable aromatic stabilization energy, while extended linear benzannelation results in increased retro-Bergman ring opening, allowing C^1-C^5 cyclization to become a competitive reaction channel.

INTRODUCTION

Intramolecular diradical cyclizations of conjugated polyunsaturated systems have become powerful additions to the arsenal of ring-forming processes.[1] The prototypical examples include C^1-C^6 Bergman[2] and C^1-C^5 Schreiner−Pascal[3] cyclizations of enediynes along with C^2-C^7 Myers−Saito[4] and C^2-C^6 Schmittel[5] cyclizations of enyne-allenes (Figure 1). In particular, Bergman cyclization has been extensively studied due to the ability of natural products such as calicheamicin and dynemicin to cleave DNA upon cyclization of an enediyne unit.[6] In addition to the development of synthetic antitumor agents,[7] diradical cyclizations have found applications as a synthetic tool in the preparation of novel polycyclic aromatic systems,[8] in the preparation of polymeric materials,[9] in the construction of molecular electronic nanodevices on surfaces,[10] and may serve as precursors to the formation of aromatic species in interstellar medium.[11] Furthermore, diradical cyclizations have provided a challenging platform toward the development of computational models due to the multiconfigurational nature of diradical species.[12]

For the parent enediyne, (*Z*)-hex-3-ene-1,5-diyne, C^1-C^6 Bergman cyclization is the preferred thermal reaction pathway, where gain of an aromatic sextet places the *p*-benzyne diradical intermediate in a deep energy well.[13] Incorporating the enediyne alkene within a benzene ring, however, increases endothermicity of C^1-C^6 cyclization as the aromaticity gain upon converting 1,2-diethynylbenzene to naphthalene is attenuated.[14] As a result, 1,2-diethynylbenzene has a lower barrier toward retro-Bergman ring opening, making cyclization to the diradical reversible.[15]

Experimentally, these energetic changes are manifested in a measured rate of disappearance for 1,2-diethynylbenzene that becomes dependent upon hydrogen atom donor concentration and provides the overall rate constant, k_{obs}, under pseudo-first-

Received: September 25, 2017
Published: November 9, 2017

DOI: 10.1021/acs.joc.7b02420
J. Org. Chem. 2017, 82, 13297−13312

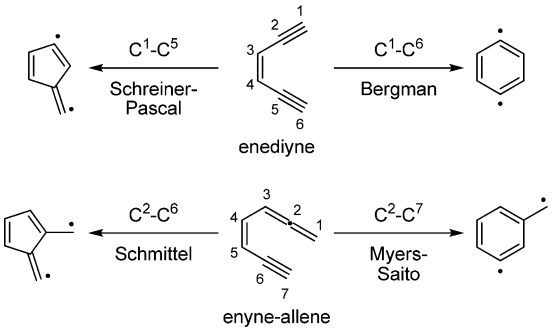

Figure 1. Diradical cyclization pathways of enediynes and enyne-allenes.

order conditions.[16] In comparison, the rate of disappearance of simple nonbenzannelated acyclic enediynes is independent of hydrogen atom donor concentration and directly provides the rate of Bergman cyclization, k_1.[17] This critical difference for benzannelated enediynes makes comparison of literature data on Bergman cyclization kinetics complicated as the concentration of hydrogen atom donor is highly variable across the available experimental data. This trend continues upon extended benzannelation as Bergman cyclization of 2,3-diethynylnaphthalene also exhibits a rate dependence on hydrogen atom donor concentration.[16] In this case, however, the measured disappearance rate is 2-fold slower compared to 1,2-diethynylbenzene with higher concentrations of hydrogen atom donor required to detect formation of cyclized product.

Unfortunately, the increased endothermic cost upon benzannelation of an enediyne cannot readily be offset through traditional substituent effects in the annealed ring. Upon C^1–C^6 cyclization, the developing diradicals are orthogonal to the π-system of the benzene ring preventing direct conjugation between radical centers and substituents. This is evident by the fact that *para*-substituents on 1,2-diethynylbenzene have minor effects on Bergman cyclization rates operating through relatively weak field effects.[18] The challenge of tuning enediyne cyclization is further complicated by the presence of two orthogonal π-systems wherein changes to the in-plane π-system (conversion to σ-bond and two radical centers) control the reaction barrier while changes to the out-of-plane π-system (gain of aromaticity) can influence overall reaction energy.[19] One approach to control the rate of Bergman cyclization of benzannelated enediynes is through reactant destabilization imparted by *ortho*-substituents.[20] Here, steric compression of the alkynes increases electron repulsion of the in-plane π-system in the reactant that is alleviated in the transition state. A more extreme route to tune enediyne reactivity through benzannelated substituents employs cyclization of enediyne radical anions.[21] Under such conditions, radical anionic cyclization of enediynes is accelerated upon benzannelation with increased sensitivity to remote substituents due to crossing of out-of-plane and in-plane molecular orbitals near the transition state. In comparison, phenyl groups located on the alkyne termini are more sensitive to substituent effects as direct conjugation to the in-plane π-system is available. For example, electron withdrawing groups present in 1,2-bis(4-nitrophenylethynyl)benzene were found to lower the C^1–C^6 activation barrier compared to electron rich *para*-methoxyphenyl substituents.[22] Overall, however, substituent effects on phenylethynyl groups have been much less studied as placement of phenyl groups on the alkyne termini significantly raises the barrier toward C^1–C^6 Bergman cyclization.[23] Furthermore, bulky phenylethynyl substituents can lead to phenyl-shifted products[24] and competing C^1–C^5 cyclization facilitated by gain of resonance stabilization to one of the radical centers from the external phenyl group.[3b]

In a previous study we reported computational data on diethynylquinoxaline isomers to further probe the influence of extended benzannelation orientation on Bergman cyclization energetics.[25] Calculations revealed that endothermicity of Bergman cyclization to the corresponding diradical intermediate can increase or decrease relative to 1,2-diethynylbenzene (ΔH_{rxn} = 9.2 kcal/mol) based on the nature of the extended aromatic core. With extended linear benzannelation, as in 6,7-diethynylquinoxaline **1** (Figure 2), Bergman cyclization

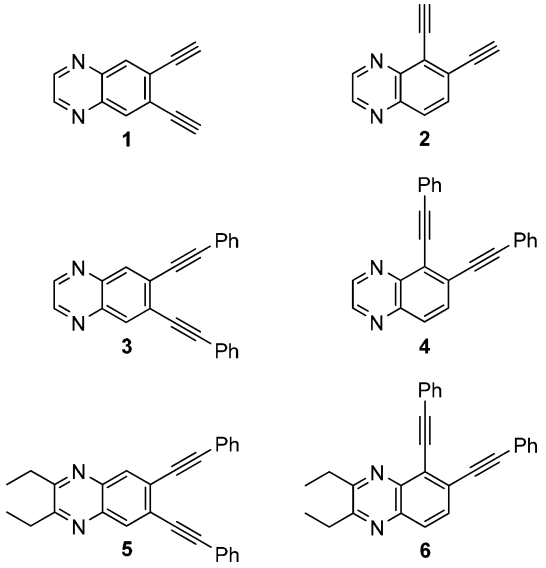

Figure 2. Quinoxalenediynes **1**–**6**.

becomes less thermodynamically favorable (ΔH_{rxn} = 12.3 kcal/mol) as the aromatic stabilization gained upon cyclization is further attenuated. In comparison, Bergman cyclization of 5,6-diethynylquinoxaline **2** is less endothermic (ΔH_{rxn} = 5.4 kcal/mol) and approaches the calculated value for (*Z*)-hex-3-ene-1,5-diyne (ΔH_{rxn} = 0.88 kcal/mol) as a new aromatic sextet is produced, restoring aromatic stabilization to the angularly fused diyl product. These results are consistent with the earlier experimental observation that 2,3-diethynylnaphthalene undergoes a more sluggish Bergman cyclization compared to 1,2-diethynylbenzene, likely due to rapid retro-Bergman cyclization.[16] Unfortunately, no experimental data is available on 1,2-diethynylnaphthalene to directly compare this effect.

Despite these changes to the reaction energy profile, aromatic or heteroaromatic cores are commonly utilized when conducting photo-Bergman cyclization[26] to prevent *cis*–*trans* isomerization of the enediyne alkene. For example, the seminal work of Turro et al.[27] and Funk et al.[28] employed benzannelated enediynes in the photocyclization of acyclic and cyclic enediynes, respectively. Subsequently, Jones et al.[29] and Hirama et al.[30] locked the central double bond within an alicyclic ring to demonstrate that aromatic cores are not strictly required for successful photo-Bergman cyclization of acyclic enediynes. Interestingly, although direct comparisons were not made, the isolated yield of photoadduct derived from 1,2-bis(phenylethynyl)cyclohexene (22%) reported by Jones is

DOI: 10.1021/acs.joc.7b02420
J. Org. Chem. 2017, 82, 13297–13312

Table 1. Relative Enthalpies[a] for C^1-C^5 Cyclization of 1−4 and Corresponding Boltzmann Percentages (cf. Structures in Figure 3)

substrate	products					
linear	**1**-*Z*	**1**-*E*	**3**-Lin			
1 (R = H)	0 (96.11%)	1.90 (3.89%)	n/a			
3 (R = Ph)	n/a	n/a	0 (100%)			
angular	**2**-*Z*	**2**-*E*	**4**-Lin	**2′**-*Z*	**2′**-*E*	**4′**-Lin
2 (R = H)	−0.27 (53.31%)	1.93 (1.30%)	n/a	0 (33.90%)	0.64 (11.49%)	n/a
4 (R = Ph)	n/a	n/a	−0.23 (59.51%)	n/a	n/a	0 (40.49%)

[a]25 °C, gas phase, kcal/mol.

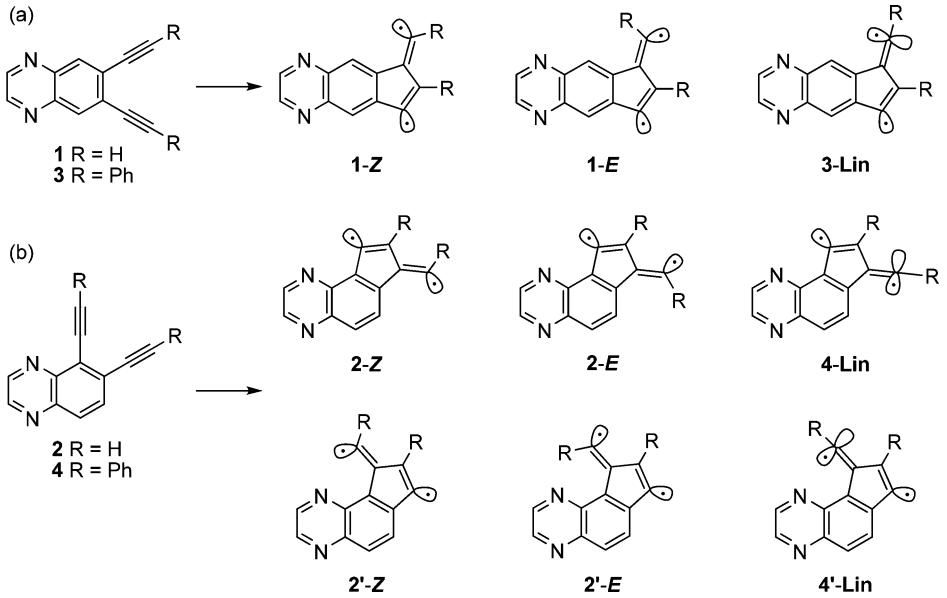

Figure 3. Isomers derived from C^1-C^5 cyclization of (a) linear quinoxalenediynes **1** and **3** and (b) angular quinoxalenediynes **2** and **4**.

higher than values typically reported for 1,2-bis-(phenylethynyl)benzene (1−10%).[24,31] Funk also noted increased conversion of an angular naphthalene-fused enediyne over the corresponding linear isomer, again suggesting aromatic stabilization can influence photo-Bergman cyclization yields. On the basis of our previous calculations, along with available literature data, the nature of extended benzannelation can provide unique opportunities to tune enediyne cyclization energetics.

In the present paper we report the syntheses, computational studies, kinetic studies, and photochemical reactivity of a series of diethynylquinoxalines to directly compare the effect of linear versus angular extended benzannelation on enediyne reactivity (Figure 2). Calculations were conducted on unsubstituted 6,7- and 5,6-diethynylquinoxalines **1** and **2** along with bis-phenylethynylquinoxaline isomers **3** and **4** to examine changes in reaction energetics along the C^1-C^6 and C^1-C^5 reaction channels. Kinetic studies, as a function of 1,4-cyclohexadiene concentration, were then conducted on terminal quinoxalenediynes **1** and **2** to gain experimental data to support our calculations. Finally, photochemical reactivity was examined on phenylethynyl quinoxalenediynes **3**−**6** to determine if a change in extended benzannelation orientation manifests in improved photo-Bergman cyclization yields for quinoxalenediynes.

RESULTS AND DISCUSSION

Computational Analysis. *A. C^1-C^5 Cyclization Products.* Prior to examining reaction energetics, relative enthalpies (Table 1) and relative free energies (Table S3) were calculated for the isomeric diyls derived from C^1-C^5 cyclization of quinoxalenediynes **1**−**4** (Figure 3). For linear derivatives **1** and **3**, symmetry in the starting enediyne leads to one possible C^1-C^5 cyclization pathway, providing a mixture of *E*/*Z* diradical intermediates. However, angular derivatives **2** and **4** lack symmetry and have two possible C^1-C^5 cyclization pathways leading to a total of four possible isomeric diradical intermediates. For terminal quinoxalenediynes **1** and **2**, the lowest energy isomers calculated for C^1-C^5 cyclization were the corresponding *Z*-diradical isomers **1**-*Z* and **2**-*Z*, respectively.[3a] For phenyl-substituted quinoxalenediynes **3** and **4**, however, optimization of the *E*/*Z* C^1-C^5 diradical isomers yielded the same structure in which the exocyclic fulvene radical adopts a virtually 180° bond angle (177.4° in **3**-**Lin**, 176.3° in **4**-**Lin**, and 174.3° in **4′**-**Lin**) leading to essentially linear intermediates which lean 3−6° toward the *Z*-isomer. As a result, optimization of isomers **1**-*Z* and **1**-*E* derived from **3** both lead to **3**-**Lin**. Similarly, optimization of **2**-*Z*/*E* and **2′**-*Z*/*E* derived from **4** provided **4**-**Lin** and **4′**-**Lin**, respectively. A similar geometrical outcome was noted by Alabugin et al. in geometry optimizations of the C^1-C^5 cyclization products derived from diaryl-substituted 1,2-diethynylbenzene derivatives.[32] The linearization of the radical center is attributed to conjugation with the terminal aryl group and consequent rehybridization of the radical center. The lowest energy isomers derived from C^1-C^5 cyclization of **1**−**4** (**1**-*Z* for **1**, **3**-**Lin** for **3**,

DOI: 10.1021/acs.joc.7b02420
J. Org. Chem. 2017, 82, 13297−13312

Table 2. Computed Cyclization Thermodynamic Parameters[a]

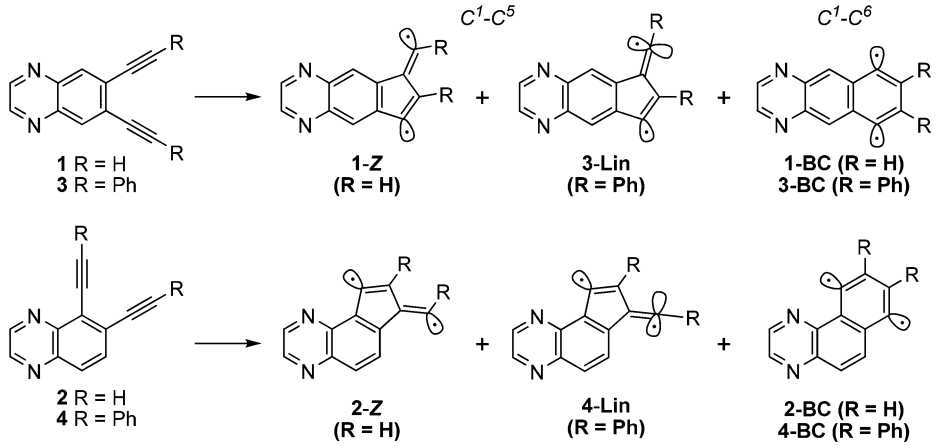

	C^1-C^5		C^1-C^6		$(C^1-C^5)-(C^1-C^6)$	
substrate	$\Delta H^{\ddagger}$	ΔH_{rxn}	$\Delta H^{\ddagger}$	ΔH_{rxn}	$\Delta\Delta H^{\ddagger}$	$\Delta\Delta H_{rxn}$
linear						
1 (R = H)	39.07	31.46	31.16	12.27	7.91	19.19
3 (R = Ph)	38.21	30.92	43.07	27.42	−4.86	3.50
angular						
2 (R = H)	40.26	32.61	30.32	5.50	9.94	27.11
4 (R = Ph)	40.16	32.68	42.36	21.11	−2.20	11.57
linear−angular						
1−**2**	−1.19	−1.15	0.84	6.77		
3−**4**	−1.95	−1.76	0.71	6.31		

[a]25 °C, gas phase, kcal/mol.

2-*Z* for **2**, and **4**-**Lin** for **4**) were then used in the computation of the cyclization reaction energetics.

B. Cyclization Reaction Energetics. To gain insight into the effect of extended benzannelation orientation and alkyne substitution pattern on C^1-C^6 and C^1-C^5 cyclization energetics, we examined activation enthalpy barriers and reaction enthalpies for quinoxalenediynes **1**−**4** computationally, with the results summarized in Table 2 (free energy barriers and reaction free energies provided in Table S1). From the data, several interesting trends emerge.

First, substitution of the terminal alkynes in **1** and **2** with phenyl groups has little effect on reaction barrier or reaction energies along the C^1-C^5 cyclization channel. Apparently, any increased steric hindrance from phenyl substitution is compensated by the gain of resonance stabilization to the developing exocyclic vinyl radical center.[3b] Upon C^1-C^6 cyclization, however, increased steric interactions from the addition of phenyl substituents cannot be offset by resonance stabilization of the developing diradical. As a result, introduction of phenyl substituents increases the C^1-C^6 activation barrier by approximately 12 kcal/mol and reaction energy by 15−16 kcal/mol for **3** and **4** compared to **1** and **2**, respectively.

Second, when comparing C^1-C^5 versus C^1-C^6 reaction pathways for unsubstituted derivatives **1** and **2**, C^1-C^6 Bergman cyclization is favored kinetically and thermodynamically. However, upon phenyl substitution in **3** and **4**, increased sterics leads to C^1-C^5 becoming the preferred reaction channel kinetically while aromatic stabilization in the C^1-C^6 product results in Bergman cyclization remaining the preferred thermodynamic reaction pathway. Overall, the thermodynamic preference for C^1-C^6 cyclization is more pronounced with the angular derivatives **2** and **4** primarily due to formation of a new aromatic sextet in these cases.[25]

Nucleus-independent chemical shift calculations (NICS (Table S4) and NICS-1 (Table 3)) confirm increased aromaticity in the newly formed 6-membered ring produced upon C^1-C^6 cyclization of the angular quinoxalenediynes compared to their linear counterparts. The NICS-1 data reveal that the new aromatic sextet generated in **2** and **4** has aromaticity 7.9% greater and 11.1% greater than the 6-membered ring formed upon C^1-C^6 cyclization of **1** and **3**, respectively. In addition, similar NICS-1 values at the transition states upon C^1-C^6 cyclization for the linear and angular analogues provide support for the small $\Delta\Delta H^{\ddagger}$ values calculated between **1** and **2** and between **3** and **4** (cf. Table 2). Furthermore, larger NICS-1 values for the C^1-C^6 cyclization products derived from **2** and **4** support larger $\Delta\Delta H_{rxn}$ values calculated between the linear and angular quinoxalenediyne derivatives. In comparison, NICS-1 calcu-

Table 3. Calculated NICS-1 Values[a] **for the 5- and 6-Membered Rings Formed in the Cyclization Reactions of 1−4**

	C^1-C^5		C^1-C^6	
substrate	transition state	product	transition state	product
1 (R = H)	−1.5	−2.2	−9.6	−11.9
2 (R = H)	−1.3	−1.9	−9.9	−12.9
3 (R = Ph)	−1.2	−1.7	−7.6	−10.2
4 (R = Ph)	−0.8	−1.3	−8.2	−11.4

[a]The NICS-1 value for the *p*-benzyne diradical singlet at the same level of theory is −12.6.

DOI: 10.1021/acs.joc.7b02420
J. Org. Chem. 2017, 82, 13297−13312

lations on the newly formed 5-membered rings produced upon C^1-C^5 cyclization of **1**–**4** confirm the negligible aromaticity gain along the C^1-C^5 reaction channel. Similar NICS and NICS-1 calculations from Schreiner et al. on (*Z*)-hex-3-ene-1,5-diyne and 1,2-diethynylbenzene likewise showed appreciable aromaticity in the Bergman cyclization transition states.[13a] Further, the decrease in the NICS-1 value from the formation of the new aromatic sextet in *p*-benzyne compared to the Bergman product formed from the benzannelated reactant 1,2-diethynylbenzene is comparable to, though somewhat smaller than, that calculated here between the Bergman cyclization of angular quinoxalenediynes **2** and **4** and linear counterparts **1** and **3**.

Finally, when examining the effect of linear versus angular extended benzannelation, the data indicates steric hindrance combined with aromatic stabilization energy can influence cyclization energetics and reaction pathway. For terminal quinoxalenediynes, derivatives **1** and **2** both favor C^1-C^6 over C^1-C^5 cyclization as the lower barrier pathway (by 7.9–9.9 kcal/mol) as well as the more energetically favorable reaction channel (by 19.2–27.1 kcal/mol). For each parameter, angular quinoxalenediyne **2** has a stronger preference for C^1-C^6 cyclization which produces a new aromatic sextet. Furthermore, for **1** and **2** the retro C^1-C^5 barrier (~7.6 kcal/mol) is significantly lower than the corresponding retro C^1-C^6 barrier (18.9–24.8 kcal/mol), with the C^1-C^6 retro-Bergman barrier of angular derivative **2** the highest retro-barrier calculated in this study, again highlighting the importance of the new aromatic sextet in the angularly fused product. Supporting this data, terminal quinoxalenediynes **1** and **2** exclusively undergo C^1-C^6 Bergman cyclization under thermal conditions (vide infra). When examining the effect of extended linear versus angular benzannelation on phenylethynyl derivatives **3** and **4**, however, the situation is not as clear. For the linear derivative **3**, addition of phenyl substituents leads to C^1-C^5 becoming the preferred kinetic pathway (favored by 4.9 kcal/mol) and, while C^1-C^6 remains the preferred thermodynamic channel (favored by 3.5 kcal/mol), attenuated aromatic stabilization gain and increased steric hindrance leads to this isomer having the smallest reaction enthalpy favoring C^1-C^6. In comparison, angular phenyl-substituted **4** has a small C^1-C^5 kinetic preference (favored by 2.2 kcal/mol), while the gain of a new aromatic sextet leads to C^1-C^6 Bergman cyclization being the preferred thermodynamic reaction channel (favored by 11.6 kcal/mol). Overall, from this data one may anticipate aromatic stabilization along the C^1-C^6 channel for angular quinoxalenediyne **4** to be the dominant energetic factor leading to a successful photo-Bergman cyclization. However, photolysis of linear quinoxalenediyne **3**, with the smallest retro-Bergman ring opening barrier, is less predictable and may lead to a mixture of cyclization products.

C. Cyclization Reaction Electronics. In addition to aromatic stabilization energy, electronic interactions between the proximal nitrogen atom and the enediyne π-orbitals or developing diyl intermediate can also influence reaction energetics for angular quinoxalenediynes.

Upon examining the reactant angular quinoxalenediynes, Mulliken charge populations reveal a small repulsion between the nitrogen atom (−0.493) and the proximal alkyne π-bond (−0.181) in angular derivative **2**. In comparison, for **4**, the charge on the nitrogen atom is nearly equal (−0.499) to that in **2**, while the charge on the proximal alkyne π-bond in **4** is significantly smaller (−0.039), leading to minimal repulsion. For both **2** and **4**, however, this electronic repulsion has little impact on the geometry of the enediyne functional group (Table 4). For example, the C^1-C^6 distances and enediyne

Table 4. Geometric Parameters for Quinoxalenediynes 1–4

substrate	C^1-C^6 distance (Å)	alkyne bond length[a] (Å)	enediyne bond angle[b]	Wiberg bond order[a]
1 (R = H)	4.126	1.208	89.90°	2.822
2 (R = H)	4.136	1.208, 1.208	89.31°	2.810, 2.817
3 (R = Ph)	4.086	1.214	90.50°	2.654
4 (R = Ph)	4.145	1.214, 1.215	89.11°	2.638, 2.646

[a]Alkyne bond lengths and bond orders are identical due to symmetry in **1** and **3**. For **2** and **4**, the alkyne proximal to the N atom is listed first. [b]Measured in the enediyne functional unit from midpoint of alkyne to midpoint of alkene to midpoint of alkyne.

bond angles (as measured from the midpoint of alkyne to midpoint of alkene to midpoint of alkyne) are nearly equal for quinoxalenediynes **1**–**4**. In addition, the alkyne bond lengths and bond orders are equal between **1** and **2** and between **3** and **4**.

To probe the effect of the nitrogen atoms on the diyl intermediates, we examined biradical stabilization energies (BSE) and singlet–triplet (S–T) splittings for quinoxalenediynes **1**–**4** along the C^1-C^5 and C^1-C^6 reaction channels (Figure 4). Close spatial proximity between the nitrogen atom and one of the radical centers in the angular diyl intermediates can affect the BSE and S–T gap,[33] each of which provide estimates of through bond coupling in the diyl.[34] As a result, any electronic effect from the proximal nitrogen atom in the angular quinoxalenediynes may be indirectly monitored by relative changes in the BSE and S–T gap compared to the linear derivative. First, the C^1-C^6 cyclization product derived from **1** has a S–T gap and BSE comparable to *p*-benzyne,[35,36] 1,4-naphthalyne,[35,36] and 5,8-quinolyne,[33] with BSE values underestimating the S–T gap as previously observed.[36] However, for the C^1-C^6 cyclization product derived from angular quinoxalenediyne **2**, both the S–T gap and BSE are lower, which suggests through space interaction between the nitrogen lone pair and the proximal radical that weakens the through bond orbital interaction between the two radical centers. The phenyl-substituted derivatives **3** and **4** similarly show a decrease in the S–T gap and BSE in going from the linear to the angular C^1-C^6 product, although the values for the S–T gap and BSE are overall smaller compared to **1** and **2**. Second, the C^1-C^5 product **1**-*Z* has a larger S–T gap and BSE compared to the C^1-C^6 product from **1** as expected due to the antiperiplanar geometry of the radical centers in **1**-*Z*.[36] In addition, the C^1-C^5 cyclization product **2**-*Z* also has a larger S–T gap and BSE versus the C^1-C^6 cyclization product from **2**. However, there is not as significant of a difference for the S–T gap and BSE between **1** and **2** along the C^1-C^5 channel compared to the C^1-C^6 channel as the distance from the proximal radical carbon to the nitrogen atom in the diradical products from **2** is 0.21 Å greater in the C^1-C^5 than in the C^1-C^6 pathway (Table 5), which minimizes any interactions. As with the C^1-C^6 reaction channel, the C^1-C^5 products **3**-**Lin** and **4**-**Lin** from the phenyl-substituted derivatives also show smaller S–T gaps and BSEs than **1**-*Z* and **2**-*Z*. However, the decrease in the S–T gap is greater than that seen along the C^1-C^6 channel upon phenyl substitution, as along the C^1-C^5 channel the exocyclic radical centers in **3**-**Lin** and **4**-**Lin**

DOI: 10.1021/acs.joc.7b02420
J. Org. Chem. 2017, 82, 13297–13312

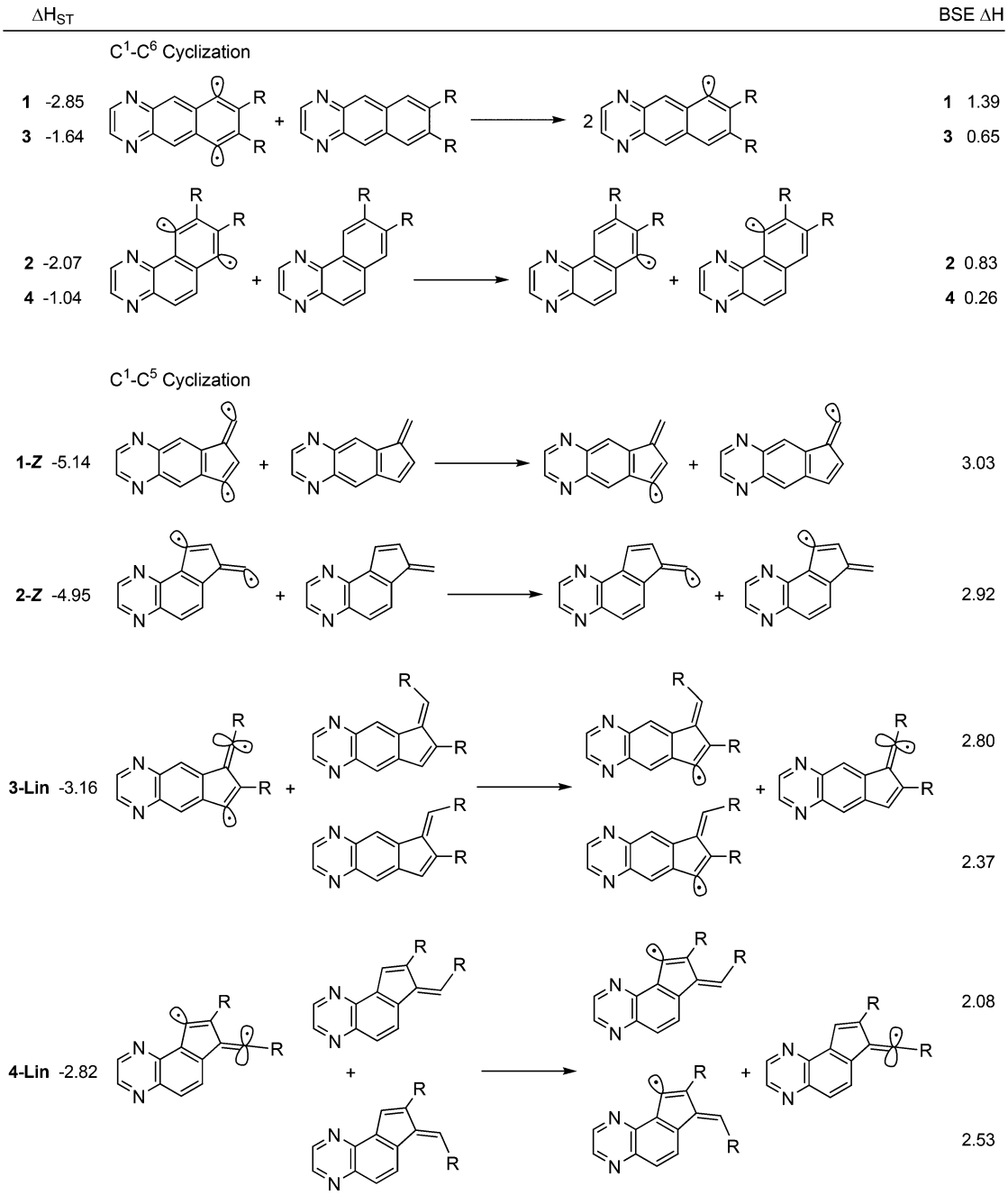

Figure 4. Singlet−triplet splitting (kcal/mol) and biradical stabilization energies (kcal/mol) of cyclization products from quinoxalenediynes **1**−**4**.

Table 5. Distance between Proximal Nitrogen Atom of the Quinoxaline Group and Carbon Radical (Å) during Cyclization Reactions of 2 and 4

	2 (R = H)	**4** (R = Ph)
C^1−C^5 TS	3.028	3.019
C^1−C^5 PRD	3.086	3.080
C^1−C^6 TS	2.856	2.860
C^1−C^6 PRD	2.878	2.888

rehybridize and gain resonance stabilization with the phenyl group, thereby reducing the through bond coupling.

The interaction between the radical sites in the diyl intermediates and the proximal nitrogen atom influences, to a small yet discernible degree, the reactivity of the angular quinoxalenediynes. For the C^1−C^6 pathway transition states and products, the Mulliken charge populations (Table 6) show that the carbon radical proximal to the nitrogen atom bears a more positive charge (difference ranging from +0.037 to +0.064) in the angularly fused cases compared to the linear analogues, while the carbon radical distal to the nitrogen atom bears a more negative charge (difference ranging from −0.015 to −0.025). This represents a small step toward zwitterionic character for the C^1−C^6 diradical[37] in the angularly fused cases, and stabilization for the slightly greater development of the cationic center is provided by the spatially aligned lone pair of the proximal nitrogen atom in the Bergman cyclization product of **2** and **4**. For **4**, this effect leads to a lower activation enthalpy ($\Delta\Delta H^{\ddagger}$ = −0.71 kcal/mol vs linear) and contributes to the lower reaction enthalpy ($\Delta\Delta H_{rxn}$ = −6.31 vs linear). In **2** though, this effect combines with the destabilization of reactant

DOI: 10.1021/acs.joc.7b02420
J. Org. Chem. 2017, 82, 13297−13312

Table 6. Mulliken Charge Populations for Carbon Radicals during Cyclization Reactions for 1−4[a]

	R = H (2)		R = H (1)		R = Ph (4)		R = Ph (3)	
	C radical proximal to N	C radical distal to N	C radical proximal to N	C radical distal to N	C radical proximal to N	C radical distal to N	C radical proximal to N	C radical distal to N
C^1−C^5 TS	0.006	−0.309	−0.032	−0.302	−0.091	0.000	−0.126	0.015
C^1−C^5 PRD	0.016	−0.221	−0.013	−0.225	−0.059	0.028	−0.088	0.033
C^1−C^6 TS	0.077	−0.012	0.013	0.013	0.001	−0.081	−0.063	−0.063
C^1−C^6 PRD	0.025	−0.036	−0.012	−0.012	−0.007	−0.066	−0.052	−0.052

[a]Data for the nitrogen proximal to the carbon radical are provided in Table S5.

Table 7. Mulliken Spin Populations for the Carbon Radicals during the Cyclization Reactions for 1−4[a]

	R = H (2)		R = H (1)		R = Ph (4)		R = Ph (3)	
	C radical proximal to N	C radical distal to N	C radical proximal to N	C radical distal to N	C radical proximal to N	C radical distal to N	C radical proximal to N	C radical distal to N
C^1−C^5 TS	−0.620	0.629	0.598	−0.620	−0.617	0.476	0.572	−0.455
C^1−C^6 TS	0.289	−0.286	0.319	−0.319	−0.589	0.583	−0.600	0.600

[a]Data for the nitrogen proximal to the carbon radical are provided in Table S5.

Scheme 1. Syntheses of Quinoxalenediynes from Dibromobenzothiadiazoles

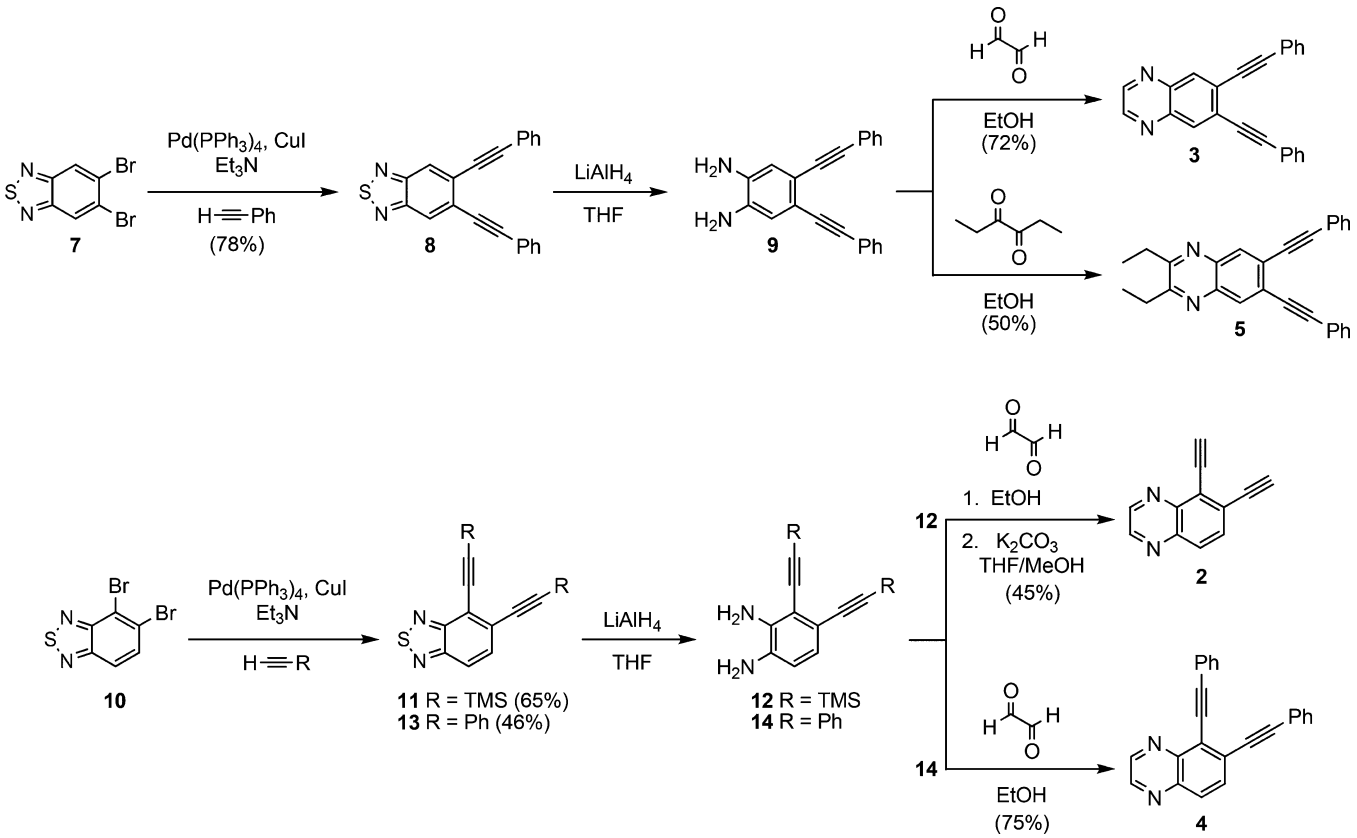

2 to give larger differences versus the linear analogue ($\Delta\Delta H^{\ddagger}$ = −0.84 kcal/mol and $\Delta\Delta H_{rxn}$ = −6.77 vs linear). The dominant energetic contribution to the $\Delta\Delta H_{rxn}$ values, though, remains aromaticity gain upon C^1−C^6 cyclization of **2** and **4**. For the C^1−C^5 pathway transition states and products, the Mulliken charge populations (Table 6) show that the carbon radical proximal to the nitrogen atom bears only a slightly more positive charge (difference ranging from +0.029 to +0.038) in the angularly fused cases compared to the linear analogues. Again, this can be explained by the greater separation between the nitrogen atom and the proximal radical center in the C^1−C^5 cyclization pathway, minimizing any stabilization of zwitterionic resonance structures by the nitrogen lone pair.

Finally, the Mulliken spin populations at the transition states (Table 7) for the radical carbons in the angularly fused C^1−C^5 reaction are larger (more so for **4** vs **3** compared to **2** vs **1**) than for the linear analogues, indicating more radical delocalization in the linear cases. The essentially identical C^1−C^5 distances in the transition states between **1** and **2** (ΔC^1−C^5 = 0.004 Å) and between **3** and **4** (ΔC^1−C^5 = 0.001 Å) suggests the spin population differences are not due to differences in timing of the transition states along the reaction coordinate. The greater spin delocalization for the linear derivatives contributes to the

DOI: 10.1021/acs.joc.7b02420
J. Org. Chem. 2017, 82, 13297−13312

C^1-C^5 cyclization becoming less kinetically favorable for **2** vs **1** ($\Delta\Delta H^{\ddagger}$ = +1.19 kcal/mol) and **4** vs **3** ($\Delta\Delta H^{\ddagger}$ = +1.95 kcal/mol), where the latter value is larger due to the greater difference in radical delocalization in **3** vs **4** compared to **1** vs **2**.

Overall, the data suggests weak interaction between the nitrogen atom and the proximal radical center in the arynes derived from angular quinoxalenediynes **2** and **4** that is more measurable along the C^1-C^6 versus C^1-C^5 channel that leads to a small increase in zwitterionic character. These effects, however, impart relatively small changes to the reaction energetics compared to aromatic stabilization energy along the C^1-C^6 channel for the angular derivatives. Future studies will more systematically examine aromatic stabilization energies and biradical stabilization energies to further refine the role of aromaticity and electronic effect imparted by nitrogen atoms on cyclization of quinoxalenediynes **1**–**4** that is beyond scope of the current paper.

Syntheses. We previously reported the synthesis and thermal C^1-C^6 cyclization of 6,7-diethynylquinoxaline **1** starting from 1,2-diiodo-4,5-dinitrobenzene.[25] In the present study two alternative synthetic routes were employed to prepare quinoxalenediynes **2**–**6** to examine kinetics and photochemical reactivity. Linear 6,7-bis(phenylethynyl)-quinoxaline derivatives **3** and **5** were prepared in three steps from commercially available 5,6-dibromo-2,1,3-benzothiadiazole **7** as outlined in Scheme 1. Sonogashira coupling[38] of **7** with phenylacetylene readily afforded benzothiadiazole **8** in 78% yield. Sulfur extrusion with $LiAlH_4$ produced diamine **9** and immediate condensation with glyoxal or 3,4-hexanedione in ethanol afforded linear quinoxalenediynes **3** and **5** in two-step yields of 72% and 50%, respectively. An analogous route was employed to generate angular derivatives 5,6-diethynylquinoxaline **2** and 5,6-bis(phenylethynyl)quinoxaline **4** from 4,5-dibromo-2,1,3-benzothiadiazole **10**.[39] Sonogashira coupling of **10** with trimethylsilylacetylene gave benzothiadiazole-based enediyne **11** in 65% yield. Subsequent treatment with $LiAlH_4$ followed by condensation with glyoxal and desilylation produced 5,6-diethynylquinoxaline **2** in a three-step 45% yield. Similarly, Sonogashira coupling between phenylacetylene and **10** gave benzothiadiazole-based enediyne **13** in 46% yield. Finally, treatment of **13** with $LiAlH_4$ and condensation with glyoxal produced angular quinoxalenediyne **4** in a two-step 75% yield.

Syntheses of quinoxalenediynes from dibromo-2,1,3-benzothiadiazole isomers is our preferred method to introduce alterations to the quinoxaline core as condensation with appropriate 1,2-dicarbonyls is conducted as the final step. In addition, we sought development of an alternative synthetic route that would employ late stage insertion of the enediyne motif more suited to modify alkyne substitution pattern in the future. This was accomplished for preparation of the angular 5,6-diethynylquinoxaline system starting from 4-amino-3-nitrophenol **15** and used to prepare quinoxalenediyne **6** as outlined in Scheme 2. Hydrogenation of **15** followed by condensation with 3,4-hexanedione afforded 2,3-diethyl-6-hydroxyquinoxaline **16** in a two-step 99% yield. Selective bromination of **16** with NBS then afforded 5-bromo-6-hydroxyquinoxaline **17** in 86% yield and treatment with *N*-phenyltriflimide gave triflate **18** in 92% yield. Finally, Sonogashira coupling of **18** with phenylacetylene provided 2,3-diethyl-5,6-bis(phenylethynyl)-quinoxaline **6** in 42% yield.

Quinoxalenediynes **1**–**6** were isolated as stable solids and purified by column chromatography or recrystallization prior to examining reactivity. Terminal quinoxalenediynes **1** and **2** were prepared to conduct kinetic studies while phenyl substituents in derivatives **3**–**6** were added to promote photochemical reactivity. Ethyl groups present in **5** and **6** were added to facilitate solubility and to prevent the potential for radical reactivity alpha to the ring nitrogen atoms (Minisci reaction[40]).

Scheme 2. Alternative Synthesis of Angular Quinoxalenediyne 6

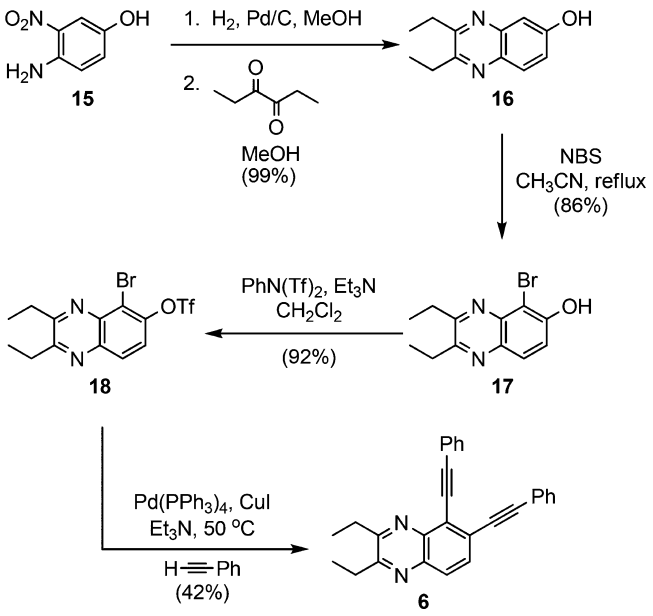

Electronic absorbance spectra for quinoxalenediynes **3**–**6** in CH_2Cl_2 were characterized by a strong absorption band between 280–300 nm with one or two lower energy absorbance bands from 360–380 nm. Finally, emission spectra of phenylethynyl quinoxalenediynes **3**–**6** gave a single broad emission band ranging from 399–449 nm, with larger Stokes shifts observed for angular isomers **4** and **6**.

Prior to examining reaction kinetics, bulk thermal cyclizations of **1** and **2** were conducted in chlorobenzene at 180 °C containing excess 1,4-cyclohexadiene (Scheme 3). For both terminal diethynylquinoxaline isomers, Bergman cyclization was the only observed reaction channel, supporting our calculations indicating C^1-C^6 cyclization is the preferred kinetic and thermodynamic pathway. For linear 6,7-diethynylquinoxaline **1**,

Scheme 3. Thermal Cyclization of Quinoxalenediynes 1 and 2

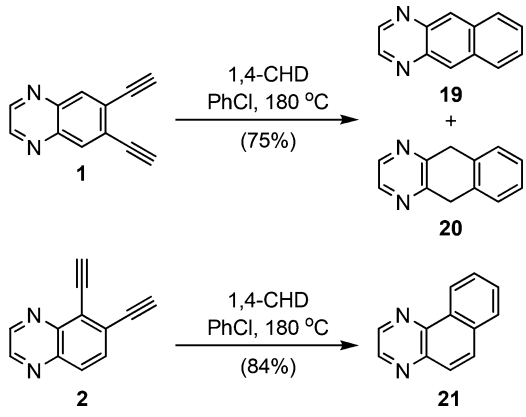

DOI: 10.1021/acs.joc.7b02420
J. Org. Chem. 2017, 82, 13297–13312

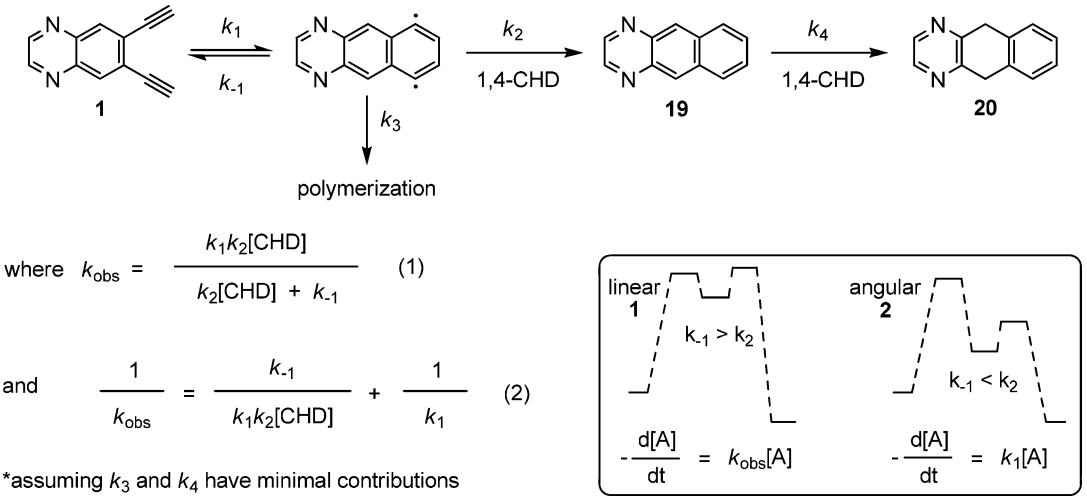

Figure 5. Kinetic model for cyclization of quinoxalenediynes (ref 42).

Table 8. Observed Rate Constants for the Disappearance of Quinoxalenediynes and Formation of Benzoquinoxalines at 180 °C[a]

substrate	[1,4-CHD] M	k_{obs} sm × 10^4	k_{obs} pdt × 10^4	k_1 × 10^4	k_{-1}/k_2
1[b]	0.258	0.505 ± 0.03	0.314 ± 0.01	7.72 ± 1.4	4.3 ± 0.9
	0.280	0.528 ± 0.03	0.378 ± 0.02		
	0.553	0.878 ± 0.04	0.860 ± 0.05		
	0.824	1.15 ± 0.03	1.23 ± 0.07		
	0.835	1.34 ± 0.08	1.39 ± 0.08		
	1.10	1.56 ± 0.07	1.60 ± 0.11		
	1.29	1.71 ± 0.05	1.74 ± 0.10		
	1.37	1.80 ± 0.08	1.86 ± 0.15		
2[c]	0.280	33.1 ± 1.5	29.8 ± 2.3	29.0 ± 1.2	
	0.410	29.0 ± 1.1	30.2 ± 2.2		
	0.600	28.0 ± 2.0	27.8 ± 1.7		

[a]Pseudo-first-order rate constants (s^{-1}) for **1**. First order rate constants (s^{-1}) for **2**. [b]Initial concentration of **1** = 5.3 × 10^{-3} M. [c]Initial concentration of **2** = 5.5 × 10^{-3} M.

however, formation of benzo[*g*]quinoxaline **19** was accompanied by slow formation of hydrogenated 5,10-dihydrobenzo[*g*]quinoxaline **20** (combined 75% yield, with pure **19** isolated in 30% yield upon DDQ oxidation of the product mixture).[25] In comparison, thermal cyclization of 5,6-diethynylquinoxaline **2** afforded benzo[*f*]quinoxaline **21** in 84% yield with no evidence of the corresponding hydrogenated product forming.

Kinetic Studies. Kinetics for **1** and **2** were followed under conditions originally described by Grissom et al.[41] and more recently modified by Alabugin et al.[42] (Figure 5). Observed rate constants for the disappearance of quinoxalenediynes and formation of benzoquinoxaline products were monitored as a function of 1,4-cyclohexadiene concentration. As described by Alabugin, monitoring the effect of 1,4-cyclohexadiene concentration on the overall reaction kinetics allows determination of k_1, the true first order rate constant for cyclization, as well as the k_{-1}/k_2 ratio graphically from eq 2 (assuming k_3 is slow in the presence of excess 1,4-cyclohexadiene and formation of hydrogenated adduct **20** from **19** is minimal).[42] Deconvolution of rate constants from the measured k_{obs} is ideally suited to examine the effect of extended benzannelation orientation on Bergman cyclization of quinoxalenediynes **1** and **2**. In the case of linear **1**, diluted aromaticity gain predicted computationally should lead to a fast retro-Bergman cyclization, with overall kinetics highly dependent on 1,4-cyclohexadiene concentration and a relatively large k_{-1}/k_2 ratio. In comparison, for angular **2** the gain of a new aromatic sextet will either render Bergman cyclization irreversible, and thus show no dependence on 1,4-cyclohexadiene concentration, or show a weaker dependence on 1,4-cyclohexadiene concentration with a smaller k_{-1}/k_2 ratio (assuming comparable k_2 values for **1** and **2**). As a result, monitoring the effect of 1,4-cyclohexadiene concentration on reaction kinetics for **1** and **2** can support our computational data and provide experimental insight into the effect of extended benzannelation orientation on Bergman cyclization energetics.

Kinetic plots monitoring the disappearance of quinoxalenediynes **1** and **2** in the presence of excess 1,4-cyclohexadiene gave good linearity monitored to 2−3 half-lives indicating first order or pseudo-first-order decay. Similarly, product formation from **1** showed excellent linearity through the first 1−2 reaction half-lives. However, at longer reaction time, product analysis was complicated by secondary formation of **20** and the kinetic significance of k_4. As a result, plots of product formation from **1** were only plotted through the first 1−2 half-lives and the small contribution of product **20** was included in the determination of total percent of product at time *t*.[43] Product analysis for **2**, which showed no indication of secondary products via transfer hydrogenation from 1,4-cyclohexadiene, gave good correlation out to 2−3 half-lives.

DOI: 10.1021/acs.joc.7b02420
J. Org. Chem. 2017, 82, 13297−13312

Observed rate constants for the disappearance of quinoxalenediynes **1** and **2** and formation of benzoquinoxaline products as a function of 1,4-cyclohexadiene concentration at 180 °C are given in Table 8. For linear isomer **1**, formation of benzoquinoxaline products gave a slower k_{obs} value compared to disappearance of starting quinoxalenediyne at low 1,4-cyclohexadiene concentration (50 equiv or less). This can be explained by significant polymerization of the diradical intermediate with k_3 becoming a kinetically significant step. At higher 1,4-cyclohexadiene concentrations (100−250 equiv) both the disappearance of quinoxalenediyne **1** and formation of cyclized products **19** and **20** showed a strong dependence on 1,4-cyclohexadiene concentration with comparable observed rate constants through the first 1−2 reaction half-lives. At longer reaction times, however, k_4 becomes significant leading to more scatter in the plots of product formation from **1**. Despite this complexity, it is clear that 6,7-diethynylquinoxaline **1** shows a strong dependence on 1,4-cyclohexadiene concentration, indicative of a reversible Bergman cyclization, as the rate of product formation increases 6-fold across the range of 1,4-cyclohexadiene concentrations examined. Finally, a plot of $1/k_{obs}$ versus 1/[CHD][44] for both quinoxalenediyne disappearance (R^2 = 0.972) and benzoquinoxaline formation (R^2 = 0.975) provided an averaged k_1 value of $7.72 \pm 1.4 \times 10^{-4}$ (s^{-1}) and a k_{-1}/k_2 ratio of 4.30 ± 0.85 for the cyclization of 6,7-diethynylquinoxaline **1** at 180 °C.

Kinetic data for angular quinoxalenediyne **2** again showed a faster rate of starting material disappearance compared to the measured rate of product formation at the lowest 1,4-cyclohexadiene concentration examined (50 equiv), indicative of polymerization. At higher 1,4-cyclohexadiene concentrations (75−100 equiv), measured rates for disappearance of quinoxalenediyne **2** and formation of benzoquinoxaline **21** were within experimental error. More importantly, disappearance of quinoxalenediyne **2** and formation of benzoquinoxaline **21** showed no dependence on hydrogen atom donor concentration as the measured rates were in excellent agreement. These results are indicative of an irreversible Bergman cyclization with the measured rate directly providing k_1. Overall, the averaged k_1 rate constant measured for Bergman cyclization of 5,6-diethynylquinoxaline **2** was $2.90 \pm 0.12 \times 10^{-3}$ (s^{-1}).

The above experimental data supports our calculations and is consistent with previous literature data in a number of ways. First, the observed change in rate-determining step from hydrogen atom abstraction for **1** to Bergman cyclization for **2** is consistent with the larger calculated retro-Bergman barrier for **2** (assuming hydrogen atom abstraction for **1** and **2** are comparable). Second, the faster k_1 rate constant measured for **2** compared to **1** supports the lower Bergman cyclization barrier calculated for **2**. Experimentally, at 180 °C k_1 is 3.8 times faster for angular derivative **2** compared to the linear isomer **1** (or $\Delta\Delta H^{\ddagger}$ = 1.20 kcal/mol). Based on our calculations (Tables S6 and S7) at 180 °C, this ratio is predicted to be 2.32:1 (or $\Delta\Delta H^{\ddagger}$ = 0.76 kcal/mol) in favor of **2**, in excellent agreement with the measured values from the kinetic studies. Third, the observed rate of disappearance of **1** at 180 °C in the presence of 100-fold excess 1,4-cyclohexadiene (8.78×10^{-5}) is significantly slower than the rate of disappearance of 1,2-diethynylbenzene reported by Alabugin et al. under identical conditions (7.83×10^{-4}).[42] Assuming comparable k_2 rates, this result is indicative of a larger k_{-1} rate constant upon linear extended benzannelation present in **1**. Furthermore, the measured k_{-1}/k_2 ratio for quinoxalenediyne **1** (4.3) is significantly larger *with* k_{-1} *becoming the dominant term* compared to k_{-1}/k_2 values measured for 3-nitro-1,2-diethynylbenzene (0.16 at 164 °C) and 4-nitro-1,2-diethynylbenzene (0.10 at 170 °C) by Alabugin.[42] Fourth, though only limited data is available to plot eq 2, the rate of thermal Bergman cyclization of 2,3-diethynylnaphthalene shows a strong 1,4-cyclohexadiene dependence similar to quinoxalenediyne **1** with a large k_{-1}/k_2 ratio (5.1 at 152 °C).[16] Finally, gain of a new aromatic sextet may explain earlier Bergman cyclization kinetic data reported in the literature including the increased reactivity of cinnolinoenediynes compared to analogous benzo-fused enediynes[45] and the absence of 1,4-cyclohexadiene concentration dependence on the rate of cyclization of imidazole-fused enediynes.[46]

The combined computational and kinetic data indicates that the retro-Bergman ring opening barrier for 6,7-diethynylquinoxaline **1** is extremely low and leads to k_{-1} becoming faster than the rate of hydrogen atom abstraction k_2. However, retro-Bergman ring opening is effectively shut down for the isomeric 5,6-diethynylquinoxaline **2** as the gain of a new aromatic sextet decreases Bergman cyclization endothermicity. Though the contribution from the nitrogen lone pair remains to be fully dissected, it is evident that extended benzannelation orientation in quinoxalenediynes **1** and **2** has a significant influence on Bergman cyclization energetics.

Photochemical Reactivity. With terminal quinoxalenediynes **1** and **2** readily undergoing thermal C^1-C^6 Bergman cyclization, we turned our attention toward photocyclization of phenylethynyl derivatives. Photochemical reactivity of quinoxalenediynes **3**−**6** was examined in a Rayonet RPR 100 reactor equipped with 16 3000 Å lamps. Initial studies were conducted on angular 5,6-bis(phenylethynyl)quinoxaline **4** in isopropanol, the most common solvent used in photo-Bergman cyclizations. Under dilute conditions, complete consumption of quinoxalenediyne **4** was observed in 4 h, providing a low and variable yield (1−5%) of C^1-C^6 cyclization product **22** (Scheme 4).

Scheme 4. Photo-Bergman Cyclization of Angular Quinoxalenediynes 4 and 6

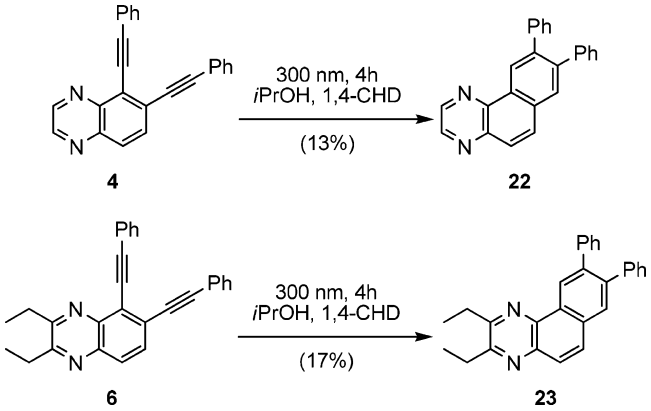

Addition of 1,4-cyclohexadiene led to more reproducible yields of benzoquinoxaline **22**, though the highest yield obtained was only marginally improved (7%). Optimal yields were obtained upon increasing reaction concentration (3 mL isopropanol per mg **4**, 200 equiv 1,4-cyclohexadiene, 4 h), providing **22** in 13% yield (based on 32% recovered quinoxalenediyne **4**). An increase in reaction time gave higher conversion of **4**, however,

DOI: 10.1021/acs.joc.7b02420
J. Org. Chem. 2017, 82, 13297−13312

Scheme 5. Photocyclization of Linear Quinoxalenediyne 3

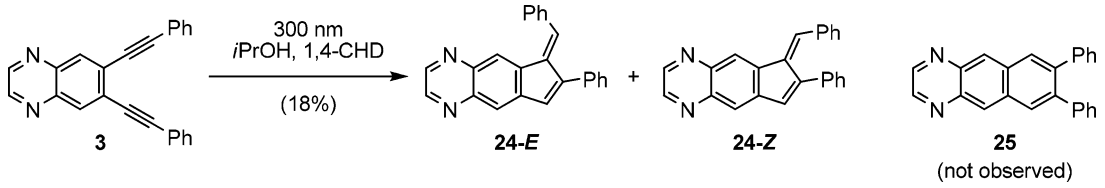

significant polymerization led to lower isolated yields of **22** upon extended irradiation. Similarly, attempts to further increase reaction concentration led to poor solubility of quinoxalenediyne **4** in isopropanol, while addition of cosolvents (acetonitrile, toluene) reduced isolated yields of **22**. Finally, with a significant absorbance band near 360 nm, photolysis of quinoxalenediyne **4** under our optimized conditions with 3500 Å lamps provided a comparable 10% yield of benzoquinoxaline **22** (based on 21% recovered starting material).

Rapid consumption of quinoxalenediyne **4** under dilute conditions, along with evidence of higher molecular weight adducts observed by GC−MS analysis, led us to speculate that radical additions alpha to the quinoxaline nitrogen atoms (Minisci reaction[40]) may contribute to rapid degradation of starting material. To limit this potential side reaction, ethyl substituents were introduced at positions 2 and 3 of the quinoxaline core in **6**. Irradiation of quinoxalenediyne **6** under our optimized conditions employed for **4** (3 mL isopropanol per mg **6**, 200 equiv 1,4-cyclohexadiene, 300 nm, 4 h) gave 49% conversion of **6** with 17% yield of benzoquinoxaline **23**, a 30% increase in yield compared to **4**. It should be noted, however, that this improved yield was primarily based on increased recovery of starting material as the isolated masses of **22** and **23** were comparable under identical conditions. For comparison, irradiation of 1,2-bis(phenylethynyl)benzene under our standard conditions afforded 2,3-diphenylnaphthalene in 9% yield (based on recovery of 10% unreacted starting material).

Photocyclization of linear analogue **3** at 300 nm under identical conditions, however, gave no evidence of C^1−C^6 Bergman cyclization product **25**. Alternatively, a 2:1 mixture of C^1−C^5 fulvene adducts, **24-*E*** and **24-*Z***, was produced in a combined 18% yield (Scheme 5). Confirming the identity of **24-*E*** and **24-*Z***, however, proved challenging as the mixture of fulvene isomers was difficult to completely separate chromatographically. Based on computational modeling, the fulvene exocyclic radical center derived from **3** (i.e., **3-Lin**) is approximately linear, supporting formation of both fulvene isomers. Furthermore, previous studies on fulvene monoradical geometries formed upon radical cyclization of 1,2-bis(phenylethynyl)benzene derivatives with AIBN/Bu_3SnH were similarly found to afford *E*/*Z*-fulvene isomers with modest stereoselectivity favoring the *E*-isomer.[32] To confirm assignment of **24-*E*** as the major isomer, computational predictions of ^{1}H NMR spectra for **24-*E*** and **24-*Z*** were conducted to compare calculated chemical shifts with experimental data. This analysis focused on the four aromatic signals of the quinoxaline core and the two vinyl hydrogens of the newly formed fulvene ring. For the major isomer, the average chemical shift deviation $\Delta\delta$ was 0.13 ppm when compared to the calculated values for **24-*E*** versus a $\Delta\delta$ value of 0.20 ppm for **24-*Z***. Likewise, the minor isomer gave a closer match to the calculated values for **24-*Z*** ($\Delta\delta$ = 0.09 ppm) versus **24-*E*** ($\Delta\delta$ = 0.22 ppm). In support of these assignments, the minor isomer showed long-range coupling between vinyl protons in the fulvene ring (^5J = 1.1 Hz) consistent with isomer **24-*Z***. Furthermore, π−π stacking of the two phenyl substituents in fulvene **24-*Z*** shifts the phenyl hydrogens upfield (7.15−6.98 ppm) compared to **24-*E*** (7.61−7.44 ppm) in agreement with calculated chemical shifts (Figure S1). Photolysis of diethyl analogue **5** under identical reaction conditions, however, produced limited quantities of C^1−C^5 products (<5%) with the bulk of starting material recovered (46%). Furthermore, separation of the fulvene product mixture derived from **5** was not possible and, as a result, full characterization was not pursued.

The change in photochemical cyclization pathway from C^1−C^6 for angular quinoxalenediynes **4** and **6** to C^1−C^5 for linear quinoxalenediyne **3** highlights the remarkable role of extended benzannelation orientation. Calculations on angular derivative **4** indicate a small kinetic preference for C^1−C^5 cyclization ($\Delta\Delta H^{\ddagger}$ = 2.2 kcal/mol favoring C^1−C^5) with a low retro-ring opening barrier ($\Delta H^{\ddagger}_{retro}$ = 7.48 kcal/mol). However, gain of a new aromatic sextet renders C^1−C^6 cyclization of quinoxalenediyne **4** the preferred thermodynamic pathway ($\Delta\Delta H_{rxn}$ = 11.57 kcal/mol in favor of C^1−C^6) with a large retro-Bergman ring opening barrier ($\Delta H^{\ddagger}_{retro}$ = 21.25 kcal/mol). Overall, our calculations and kinetic data are in agreement with the observed photochemical reactivity of angular quinoxalenediynes **4** and **6** that produce C^1−C^6 benzoquinoxalines **22** and **23**, respectively. In comparison, calculations on linear derivative **3** indicate a much smaller thermodynamic preference for C^1−C^6 cyclization ($\Delta\Delta H_{rxn}$ = 3.50 kcal/mol) with a lower retro-Bergman ring opening barrier ($\Delta H^{\ddagger}_{retro}$ = 15.65 kcal/mol) due to reduced aromatic stabilization energy gained in the linearly fused product. Furthermore, kinetic data on linear quinoxalenediyne **1** suggests retro-Bergman ring opening will predominate over hydrogen atom abstraction upon C^1−C^6 cyclization of **3** and **5**. With no strong C^1−C^6 thermodynamic driving force, coupled with a larger kinetic preference for C^1−C^5 cyclization ($\Delta\Delta H^{\ddagger}$ = 4.86 kcal/mol favoring C^1−C^5), photocyclization of linear quinoxalenediyne **3** leads to exclusive formation of C^1−C^5 fulvenes **24-*E*** and **24-*Z***. While a change in reaction pathway from C^1−C^6 Bergman to C^1−C^5 Schreiner-Pascal cyclization has precedence,[36] this change is typically the result of increased steric hindrance for enediynes (as well as enyne-allenes[47]) as opposed to reduced aromatic stabilization energy observed in the current model. The exact nature of how C^1−C^5 products are produced from quinoxalenediyne **3**, however, is unclear. While our calculations indicate direct C^1−C^5 cyclization is a viable reaction pathway, radical addition reactions can also contribute to formation of fulvenes **24-*E*** and **24-*Z***.[32,48,49]

The combined computational and experimental data indicate extended benzannelation orientation can readily influence photochemical reactivity of acyclic phenylethynyl enediynes. With extended angular benzannelation in quinoxalenediynes **4** and **6**, an irreversible C^1−C^6 photo-Bergman cyclization is favored exclusively as a new aromatic sextet is produced. On the other extreme, diluted aromaticity gain upon C^1−C^6 cyclization of quinoxalenediyne **3** possessing extended linear

DOI: 10.1021/acs.joc.7b02420
J. Org. Chem. 2017, 82, 13297−13312

benzannelation effectively shuts down photo-Bergman cyclization. As a result, alternative reaction pathways, such as C^1-C^5 cyclization, become feasible for **3** that are not observed in photocyclization of **4** and **6**.

CONCLUSION

The above work describes a combined computational and experimental study on 5,6-diethynylquinoxaline and 6,7-diethynylquinoxaline derivatives to examine the effect of angular versus linear extended benzannelation on C^1-C^5 and C^1-C^6 cyclization channels of enediynes.

With extended linear benzannelation, 6,7-diethynylquinoxaline **1** has a slower rate of thermal Bergman cyclization compared to 1,2-diethynylbenzene derivatives and angular 5,6-diethynylquinoxaline **2**. This can be rationalized by a lower retro-Bergman ring opening barrier for 6,9-benzo[*g*]-quinoxalyne, formed upon C^1-C^6 cyclization of **1**, as ring opening of this aryne intermediate does not suffer from a large loss of aromatic stabilization. As a result, the rate of cyclization of **1** is highly dependent upon the concentration of hydrogen atom donor, with the rate of retro-Bergman ring opening four times faster than the rate of hydrogen atom abstraction. Calculations support the observed experimental data with increased enthalpy barrier and reaction enthalpy for C^1-C^6 cyclization of **1** compared to **2**. Furthermore, NICS calculations confirm decreased aromatic stabilization upon C^1-C^6 Bergman cyclization of linear quinoxalenediyne **1** compared to **2**. Finally, with diluted aromaticity gain and rapid retro-Bergman ring opening, photolysis of linear phenylethynyl-substituted quinoxalenediyne **3** leads to C^1-C^5 Schreiner–Pascal cyclization to fulvene adducts, the kinetically favored pathway based on calculations and the primary reaction channel observed.

In contrast, thermal Bergman cyclization of 5,6-diethynylquinoxaline **2**, with extended angular benzannelation, is irreversible and the rate independent of hydrogen atom donor concentration as observed for simple nonbenzannelated enediynes. NICS calculations support increased gain in aromatic stabilization energy in the angular 7,10-benzo[*f*]-quinoxalyne intermediate as the primary factor to rationalize the decreased cyclization endothermicity and increased retro-Bergman ring opening barrier calculated for **2**. Finally, with restored aromatic stabilization, phenylethynyl-substituted quinoxalenediynes **4** and **6** show modest improvement in C^1-C^6 photo-Bergman cyclization yields compared to 1,2-bis-(phenylethynyl)benzene.

Calculated singlet–triplet splittings and biradical stabilization energies indicate increased interaction between the proximal nitrogen atom and the radical center in the aryne intermediate derived from angular quinoxalenediynes **2** and **4**. While this may play a small role on overall reaction energetics, studies to further define the role of the nitrogen atom on cyclization channels of quinoxalenediynes and related naphthalenediynes are under investigation.

These results suggest a modification to the current model used to predict kinetics of Bergman cyclization, which simply states that benzannelation alters the rate limiting step, to the following; generation of a new aromatic sextet renders C^1-C^6 Bergman cyclization of enediynes irreversible. This new model may be equally applied to simple cyclic and acyclic enediynes, benzannelated enediynes, heteroaromatic enediynes, enediynes fused to nonbenzenoid aromatic rings and enediynes fused to extended aromatic systems.

Finally, the contrasting photochemical reactivity of linear quinoxalenediyne **3** compared to angular quinoxalenediynes **4** and **6** provides an interesting example wherein a change in reaction pathway occurs due to energetic considerations of the aryne intermediates as opposed to steric considerations of the enediyne reactant. With the majority of photoactivated enediynes described in the literature derived from simple benzannelated enediynes, altering the extent and orientation of benzannelation may provide a route to design more efficient acyclic enediynes for photo-Bergman cyclization.

EXPERIMENTAL SECTION

Computational Methodology. All calculations were carried out with the Gaussian 09 quantum chemistry program.[50] The mPW1PW91 functional[51,52] has been shown to accurately reproduce crystal structures of arenediynes[23] as well as C^1-C^6 activation and reaction enthalpies for parent compounds (*Z*)-hex-3-ene-1,5-diyne and 1,2-diethynylbenzene,[25] and was therefore used for the calculations involving quinoxalenediynes **1**–**4**. Geometry optimizations utilized the 6-31G(d,p) basis set, and single-point energies for all stationary points utilized the cc-pVTZ basis set. Calculations were carried out in the gas phase as reaction energetics for Bergman cyclization are not significantly affected by the inclusion of solvation energies.[25] Restricted wave functions were utilized for the close-shell reactant quinoxalenediynes. Calculations for the cyclization transition states and diradical products were carried out with broken-symmetry unrestricted wave functions due to the open-shell character of these species.[3a,12a] Vibrational frequency calculations enabled verification of the stationary points as well as tabulation of zero-point energy, thermal enthalpy, and thermal entropy corrections, enabling reaction enthalpies and reaction free energies to be calculated. Singlet and triplet states were calculated for the transition states and diradical products. As all singlet states proved to be lower in energy than the triplet states (Table S2), singlet states are used as the focus of the Results and Discussion.

Nucleus-independent chemical shifts (NICS) were used to measure the aromaticity of the newly formed rings in the singlet transition states and singlet products of the cyclization reactions.[53] The NICS values are calculated at the geometric center of the rings, as determined by averaging the Cartesian coordinates of the carbon atoms comprising the ring. NICS-1 values were also calculated, in which the NICS position was exactly 1 Å above the center of the ring plane.[13a,54] The NICS-1 values are affected mainly by π contributions, with minimal contributions from the C–C and C–H σ bonds. The NICS calculations used the geometries optimized with the mPW1PW91 functional and the 6-31G(d,p) basis set and are calculated using the same functional with the larger 6-311++G(d,p) basis set needed for accurate NMR calculations.[55]

Biradical stabilization energies (BSE) are calculated via isodesmic reactions for the hydrogen transfer to the singlet diradical from the corresponding closed-shell species to give a pair of monoradicals. BSE calculations are carried out at the same level of theory used for the cyclization reaction energetics. The enthalpy changes (including zero-point energy and thermal enthalpy corrections) for the isodesmic reactions represent the BSE values for the singlet diradicals. Positive BSEs are indicative of stabilization, while negative BSEs imply destabilization, between two radical sites in the same molecule.

^{1}H and ^{13}C chemical shifts were calculated using density functional theory methods according to the procedure from Wiitala et al.[56] Specifically, geometries were first optimized at the B3LYP/6-31G(d) level with chloroform as the solvent (IEF-PCM solvation method). NMR chemical shifts were then calculated in chloroform solvent at the B3LYP/6-311+G(2d,p) level. Chemical shifts relative to TMS were then corrected according to the linear regression formulas given by Wiitala et al. (^{1}H: actual = 0.9333 × calculated + 0.1203; ^{13}C: actual = 0.9488 × calculated − 2.1134), who developed this method for application to chemical shifts calculated in chloroform solvent in order to correct for systematic errors in the calculated chemical shift values. Relative enthalpies and free energies for the C^1-C^5 product isomers

DOI: 10.1021/acs.joc.7b02420
J. Org. Chem. 2017, 82, 13297–13312

from cyclization of **3** and **4** (Tables S8 and S9) were computed from the single point energies obtained in chloroform solvent at the B3LYP/6-311+G(2d,p) level and include zero-point energy, thermal enthalpy, and thermal entropy corrections.

General Procedures. All reagents and solvents were obtained from commercial suppliers and used without further purification. 6,7-diethynylquinoxaline **1**,[25] benzo[*g*]quinoxaline **19**,[25] and 4,5-dibromo-2,1,3-benzothiadiazole **10**[39] were prepared as previously described. Air sensitive reactions were performed under an inert atmosphere of argon. TLC was performed on precoated silica plates and visualized with short- and long-wavelength UV light. Flash chromatography was conducted with 230−400 mesh silica gel packed in glass columns with the indicated solvent system. Thermolysis reactions were conducted in an oil bath equipped with a temperature controller. Photochemical reactions were conducted in a quartz vessel with a Rayonet photochemical reactor equipped with 16 300 or 350 nm lamps. Melting points were determined in open capillary tubes on a Mel-Temp apparatus and are uncorrected. ^{1}H and ^{13}C NMR spectra were recorded on a 500 MHz spectrometer and are reported in ppm relative to tetramethylsilane (0.0 ppm) for ^{1}H or $CDCl_3$ (77.0 ppm) for ^{13}C. FTIR spectra were obtained as a thin film with a diamond ATR accessory. UV−visible absorbance and emission spectra were obtained on air-equilibrated CH_2Cl_2 solutions at 20−25 °C. Mass spectra were recorded using electrospray ionization with a time-of-flight or Fourier transform ion cyclotron resonance mass analyzer.

Kinetic Studies. Separate stock solutions of quinoxalenediyne **1** (10.6 mM) and **2** (11.0 mM) in chlorobenzene were prepared in 5 mL volumetric flasks containing naphthalene (10 mM) as an internal standard. 1.0 mL aliquots of these stock solutions were transferred to 2.0 mL volumetric flasks which contained 50−250 mol equiv of 1,4-cyclohexadiene. The volumetric flasks were filled to the mark to deliver final solutions that were 5.0 mM naphthalene internal standard, 0.258−1.37 M 1,4-cyclohexadiene, and 5.3 mM quinoxalenediyne **1** or 5.5 mM quinoxalenediyne **2**. 50 μL of the new 1,4-cyclohexadiene stock solutions were transferred to 10−15 capillary melting point tubes that were frozen in liquid nitrogen and flame-sealed leaving enough head space for liquid expansion to fill the capillary tube upon heating. The capillary tubes were then placed on a wire mesh submerged in a preheated oil bath at 180 ± 1 °C and monitored out to 2−3 half-lives. Samples were removed at regular time intervals, immediately cooled in an ice−water bath, and analyzed by GC-FID. The GC used the following temperature ramp: initial temperature 100 °C for 2 min, ramp 15 °C per minute to 250 °C and hold for 10 min; retention time naphthalene internal standard = 1.2 min, quinoxalenediyne **1** = 5.0 min, benzo[*g*]quinoxaline **19** = 6.4 min, 5,10-dihydrobenzo[*g*]-quinoxaline **20** = 5.6 min, quinoxalenediyne **2** = 5.3 min, and benzo[*f*]quinoxaline **21** = 5.9 min. The percent starting material and product, relative to internal standard, were determined from area counts. For quinoxalenediyne **1**, two products are produced (benzo[*g*]quinoxaline **19** and dihydrobenzo[*g*]quinoxaline **20**) and the percent of each product was determined with the sum of the two products used in the kinetic plots which leads to more scatter in the plots of product formation from quinoxalenediyne **1** at longer time. Each sample was analyzed by GC a minimum of three times to provide relative standard deviations of 5% or less for the averaged percent starting material remaining and percent product formed. For starting material disappearance, a plot of $\ln(A/A_0)$ versus time provided k_{obs} where A_0 is the initial percent of starting material relative to naphthalene internal standard and A is the percent of starting material at time t. For product formation, a plot of $\ln(P_\infty/(P_\infty - P))$ versus time provided k_{obs} where P_∞ is the final percent of product relative to naphthalene internal standard and P is the percent of product at time t (Figures S5 and S7 for quinoxalenediynes **1** and **2**, respectively). Errors in the measured k_{obs} values are standard deviations of the line fits with 95% confidence limits. For quinoxalenediyne **1**, a plot of $1/k_{obs}$ versus 1/[CHD] provided k_1 and the k_{-1}/k_2 ratio (Figure S6).

*5,6-Bis(phenylethynyl)benzo[c][1,2,5]thiadiazole (**8**).* To an argon degassed solution of 7 (1.50 g, 5.10 mmol) in 1:1 THF/Et_3N (60 mL) was added copper iodide (0.039 g, 0.205 mmol), phenylacetylene (1.56 g, 15.3 mmol) and tetrakis (triphenylphosphine)palladium(0) (0.236 g, 0.204 mmol) and the resulting solution was stirred under argon in the dark for 5 h at 50 °C. Upon completion the reaction mixture was diluted with CH_2Cl_2, washed with saturated aqueous NH_4Cl, saturated aqueous NaCl, dried (Na_2SO_4) and evaporated in vacuo. The resulting solids were recrystallized (ethanol) to give **8** as a brown solid (1.34 g, 78%): mp 150−151 °C; ^{1}H NMR (500 MHz, $CDCl_3$) δ 8.25 (s, 2H), 7.65−7.63 (m, 4H), 7.44−7.38 (m, 6H); ^{13}C NMR (125 MHz, $CDCl_3$) δ 153.9, 131.9, 129.0, 128.5, 126.7, 124.3, 122.7, 96.2, 87.4; IR (ATR) cm^{-1} 2212, 1597, 1495; HRMS (ESI-TOF) m/z [M + H]$^+$ Calcd for $C_{22}H_{13}N_2S$ 337.0794; Found 337.0801.

*6,7-Bis(phenylethynyl)quinoxaline (**3**).* To a solution of **8** (0.658 g, 1.96 mmol) in THF (11 mL) at 0 °C was added $LiAlH_4$ (3.1 mL of 2.5 M solution in THF, 7.8 mmol) and the resulting solution allowed to warm to room temperature over 30 min. Upon completion the reaction mixture was diluted with wet ether and washed with water, saturated aqueous NH_4Cl, saturated aqueous NaCl, dried (Na_2SO_4) and evaporated in vacuo. The resulting dark red oil was immediately dissolved in ethanol (10 mL), glyoxal (0.291 g of 40 wt %/wt solution in water, 2.00 mmol) was added, and the solution allowed to stir overnight. Upon completion the reaction mixture was concentrated in vacuo and purified by recrystallization (ethanol) to afford **3** as a tan solid (0.468 g, 72%): mp 140−141 °C; ^{1}H NMR (500 MHz, $CDCl_3$) δ 8.85 (s, 2H), 8.31 (s, 2H), 7.67−7.64 (m, 4H), 7.44−7.38 (m, 6H); ^{13}C NMR (125 MHz, $CDCl_3$) δ 145.8, 142.4, 132.6, 131.9, 129.0, 128.5, 127.2, 122.7, 95.9, 87.4; IR (ATR) cm^{-1} 2220, 1604, 1501; UV−vis (CH_2Cl_2) λ_{max} (nm) (log ε) 300 (4.77), 366 (4.08), 384 (4.04); Em (CH_2Cl_2; excitation 350 nm) λ_{max} (nm) 409; HRMS (ESI-TOF) m/z [M + H]$^+$ Calcd for $C_{24}H_{15}N_2$ 331.1230; Found 331.1232.

*2,3-Diethyl-6,7-bis(phenylethynyl)quinoxaline (**5**).* To a solution of **8** (0.646 g, 1.92 mmol) in THF (11 mL) at 0 °C was added $LiAlH_4$ (3.1 mL of 2.5 M solution in THF, 7.78 mmol) and the resulting solution allowed to warm to room temperature over 30 min. Upon completion the reaction mixture was diluted with wet ether and washed with water, saturated aqueous NH_4Cl, saturated aqueous NaCl, dried (Na_2SO_4) and evaporated in vacuo. The resulting dark red oil was immediately dissolved in ethanol (10 mL), 3,4-hexanedione (0.219 g, 1.92 mmol) was added, and the solution allowed to stir overnight. Upon completion the reaction mixture was concentrated in vacuo and purified by recrystallization (ethanol) to afford **5** as a tan solid (0.372 g, 50%): mp 169−171 °C; ^{1}H NMR (500 MHz, $CDCl_3$) δ 8.23 (s, 2H), 7.65−7.63 (m, 4H), 7.40−7.39 (m, 6H), 3.07 (q, J = 7.5 Hz, 4H), 1.45 (t, J = 7.4 Hz, 6H); ^{13}C NMR (125 MHz, $CDCl_3$) δ 158.4, 140.4, 132.0, 131.8, 128.7, 128.4, 125.6, 123.1, 94.6, 87.9, 28.4, 12.1; IR (ATR) cm^{-1} 2209, 1609, 1493; UV−vis (CH_2Cl_2) λ_{max} (nm) (log ε) 298 (4.80), 365 (4.08), 379 (4.09); Em (CH_2Cl_2; excitation 350 nm) λ_{max} (nm) 399; HRMS (ESI-TOF) m/z [M + H]$^+$ Calcd for $C_{28}H_{23}N_2$ 387.1856; Found 387.1858.

*4,5-Bis((trimethylsilyl)ethynyl)benzo[c][1,2,5]thiadiazole (**11**).* To an argon degassed solution of **10** (0.530 g, 1.80 mmol) in 1:1 THF/Et_3N (40 mL) was added copper iodide (0.013 g, 0.068 mmol), trimethylsilylacetylene (0.534 g, 5.44 mmol) and tetrakis (triphenylphosphine)palladium(0) (0.082 g, 0.071 mmol) and the resulting solution was stirred under argon in the dark for 8 h at 50 °C. Upon completion the reaction mixture was diluted with CH_2Cl_2, washed with saturated aqueous NH_4Cl, saturated aqueous NaCl, dried (Na_2SO_4) and evaporated in vacuo. The resulting solids were recrystallized (methanol) to give **11** as a yellow solid (0.382 g, 65%): mp 68−70 °C; ^{1}H NMR (500 MHz, $CDCl_3$) δ 7.87 (d, J = 9.1 Hz, 1H), 7.62 (d, J = 9.1 Hz, 1H), 0.36 (s, 9H), 0.32 (s, 9H); ^{13}C NMR (125 MHz, $CDCl_3$) δ 154.5, 153.8, 132.8, 127.8, 121.1, 119.5, 106.9, 103.9, 102.7, 99.0, 0.04, −0.09; IR (ATR) cm^{-1} 2144, 1579, 1512; HRMS (ESI-FTICR) m/z [M + H]$^+$ Calcd for $C_{16}H_{21}N_2SSi_2$ 329.0959; Found 329.0959.

*5,6-Diethynylquinoxaline (**2**).* To a solution of **11** (0.364 g, 1.11 mmol) in THF (8 mL) at 0 °C was added $LiAlH_4$ (1.4 mL of 2.5 M solution in THF, 3.5 mmol) and the resulting solution allowed to warm to room temperature over 30 min. Upon completion the reaction mixture was diluted with wet ether and washed with water, saturated aqueous NH_4Cl, saturated aqueous NaCl, dried (Na_2SO_4)

DOI: 10.1021/acs.joc.7b02420
J. Org. Chem. 2017, 82, 13297−13312

and evaporated in vacuo. The resulting dark red oil was immediately dissolved in ethanol (10 mL), glyoxal (0.272 g of 40 wt %/wt solution in water, 1.88 mmol) was added, and the solution allowed to stir overnight. Upon completion the reaction mixture was concentrated in vacuo, dissolved in THF (10 mL) and a saturated solution of K_2CO_3 in methanol (2 mL) was added. Upon stirring 1 h, the reaction mixture was concentrated in vacuo and purified by flash column chromatography (9:1 dichloromethane/ethyl acetate) to afford **2** as a brown solid (0.089 g, 45%): mp 166−168 °C (d); ^{1}H NMR (500 MHz, $CDCl_3$) δ 9.00 (d, J = 1.8 Hz, 1H), 8.89 (d, J = 1.8 Hz, 1H), 8.07 (d, J = 8.8 Hz, 1H), 7.85 (d, J = 8.8 Hz, 1H), 3.91 (s, 1H), 3.62 (s, 1H); ^{13}C NMR (125 MHz, $CDCl_3$) δ 146.0, 145.7, 143.4, 142.6, 132.9, 130.1, 128.1, 125.7, 88.4, 84.8, 81.5, 78.7; IR (ATR) cm^{-1} 3222, 2098, 1595, 1490; UV−vis (CH_2Cl_2) λ_{max} (nm) (log ε) 258 (4.49), 262 (4.52), 330 (3.76); Em (CH_2Cl_2; excitation 350 nm) λ_{max} (nm) 428; HRMS (ESI-FTICR) m/z [M + H]$^+$ Calcd for $C_{12}H_7N_2$ 179.0604; Found 179.0604.

*4,5-Bis(phenylethynyl)benzo[c][1,2,5]thiadiazole (**13**).* To an argon degassed solution of **10** (1.00 g, 3.40 mmol) in 1:1 THF/Et_3N (60 mL) was added copper iodide (0.026 g, 0.137 mmol), phenylacetylene (1.04 g, 10.2 mmol) and tetrakis (triphenylphosphine)palladium(0) (0.157 g, 0.136 mmol) and the resulting solution was stirred under argon in the dark for 5 h at 50 °C. Upon completion the reaction mixture was diluted with CH_2Cl_2, washed with saturated aqueous NH_4Cl, saturated aqueous NaCl, dried (Na_2SO_4) and evaporated in vacuo. The resulting solids were purified by flash column chromatography (9:1 hexanes/ethyl acetate) to give **13** as a yellow solid (0.521 g, 46%): mp 125−126 °C; ^{1}H NMR (500 MHz, $CDCl_3$) δ 7.96 (d, J = 9.1 Hz, 1H), 7.76 (d, J = 9.1 Hz, 1H), 7.75−7.74 (m, 2H), 7.67−7.65 (m, 2H), 7.45−7.40 (m, 6H); ^{13}C NMR (125 MHz, $CDCl_3$) δ 154.6, 154.0, 132.6, 132.1, 131.9, 129.2, 129.1, 128.6, 128.5, 127.4, 122.8, 122.7, 120.9, 119.4, 100.8, 98.0, 88.2, 84.9; IR (ATR) cm^{-1} 2256, 1587, 1497; HRMS (ESI-TOF) m/z [M + H]$^+$ Calcd for $C_{22}H_{13}N_2S$ 337.0794; Found 337.0789.

*5,6-Bis(phenylethynyl)quinoxaline (**4**).* To a solution of **13** (0.300 g, 0.892 mmol) in THF (10 mL) at 0 °C was added $LiAlH_4$ (1.4 mL of 2.5 M solution in THF, 3.50 mmol) and the resulting solution allowed to warm to room temperature over 30 min. Upon completion the reaction mixture was diluted with wet ether and washed with water, saturated aqueous NH_4Cl, saturated aqueous NaCl, dried (Na_2SO_4) and evaporated in vacuo. The resulting dark red oil was immediately dissolved in ethanol (10 mL), glyoxal (0.145 g of 40 wt %/wt solution in water, 1.00 mmol) was added, and the solution allowed to stir overnight. Upon completion the reaction mixture was concentrated in vacuo and purified by recrystallization (ethanol) to afford **4** as a yellow solid (0.220 g, 75%): mp 145−146 °C; ^{1}H NMR (500 MHz, $CDCl_3$) δ 9.01 (d, J = 1.8 Hz, 1H), 8.88 (d, J = 1.8 Hz, 1H), 8.06 (d, J = 8.8 Hz, 1H), 7.93 (d, J = 8.7 Hz, 1H), 7.77−7.75 (m, 2H), 7.66−7.64 (m, 2H), 7.41−7.39 (m, 6H); ^{13}C NMR (125 MHz, $CDCl_3$) δ 145.8, 145.2, 143.3, 142.6, 132.7, 132.1, 131.9, 129.2, 129.1, 128.9, 128.6, 128.5, 128.4, 126.2, 123.2, 122.8, 101.1, 97.3, 88.4, 85.6; IR (ATR) cm^{-1} 2206, 1609, 1499; UV−vis (CH_2Cl_2) λ_{max} (nm) (log ε) 282 (4.63), 287 (4.63), 364 (4.21); Em (CH_2Cl_2; excitation 350 nm) λ_{max} (nm) 449; HRMS (ESI-TOF) m/z [M + H]$^+$ Calcd for $C_{24}H_{15}N_2$ 331.1230; Found 331.1230.

*2,3-Diethylquinoxalin-6-ol (**16**).* To a solution of 4-amino-3-nitrophenol **15** (2.51 g, 16.3 mmol) in methanol (125 mL) was added 5% palladium on carbon (0.518 g) and the mixture was stirred under an atmosphere of hydrogen in the dark overnight. Upon completion as judged by TLC, the reaction mixture was filtered through Celite, degassed with argon, and 3,4-hexanedione (1.86 g, 16.3 mmol) was added. After stirring in the dark overnight the solution was concentrated in vacuo to afford **16** as a dark brown solid pure by ^{1}H NMR (3.25 g, 99%): mp 165−167 °C; ^{1}H NMR (500 MHz, $CDCl_3$) δ 9.91 (br s, 1H), 7.64 (d, J = 9.1 Hz, 1H), 7.19 (d, J = 2.6 Hz, 1H), 6.95 (dd, J = 9.1, 2.6 Hz, 1H); 3.04 (q, J = 7.5 Hz, 2H), 2.98 (q, J = 7.6 Hz, 2H), 1.46 (t, J = 7.5 Hz, 3H), 1.36 (t, J = 7.6 Hz, 3H); ^{13}C NMR (125 MHz, $CDCl_3$) δ 157.5, 156.7, 154.10, 140.9, 136.4, 129.8, 121.0, 107.9, 28.1, 28.0, 13.1, 13.0; IR (ATR) cm^{-1} 3082 (br OH), 1620, 1457; HRMS (ESI-TOF) m/z [M + H]$^+$ Calcd for $C_{12}H_{15}N_2O$ 203.1179; Found 203.1176.

*5-Bromo-2,3-diethylquinoxalin-6-ol (**17**).* To a suspension of **16** (0.752 g, 3.72 mmol) in acetonitrile (15 mL) was added N-bromosuccinimide (0.662 g, 3.72 mmol) and the resulting solution was refluxed for 30 min. An additional portion of N-bromosuccinimide (0.166 g, 0.933 mmol) was added and the solution refluxed an additional 30 min. Upon completion as judged by TLC, the reaction mixture was cooled to room temperature, poured onto ice, and vacuum filtered to afford **17** as a brown solid pure by ^{1}H NMR (0.895 g, 86%): mp 126−128 °C; ^{1}H NMR (500 MHz, $CDCl_3$) δ 7.89 (d, J = 9.1 Hz, 1H), 7.44 (d, J = 9.1 Hz, 1H), 6.20 (s, 1H); 3.08 (q, J = 7.4 Hz, 2H), 3.03 (q, J = 7.5 Hz, 2H), 1.47 (t, J = 7.4 Hz, 3H), 1.39 (t, J = 7.5 Hz, 3H); ^{13}C NMR (125 MHz, $CDCl_3$) δ 158.0, 155.2, 153.1, 139.1, 137.2, 128.9, 119.3, 106.7, 28.2, 27.8, 12.5, 12.0; IR (ATR) cm^{-1} 2583 (br OH), 1613, 1448; HRMS (ESI-TOF) m/z [M + H]$^+$ Calcd for $C_{12}H_{14}BrN_2O$ 281.0284; Found 281.0289.

*5-Bromo-2,3-diethylquinoxalin-6-yl trifluoromethanesulfonate (**18**).* To a suspension of **17** (0.558 g, 1.99 mmol) in CH_2Cl_2 (10 mL) was added Et_3N (1.22 g, 12.1 mmol) and the resulting suspension was cooled to 0 °C. $PhN(Tf)_2$ (0.745 g, 2.09 mmol) was added and the solution stirred at 0 °C for 1 h. Upon completion as judged by TLC, the reaction mixture was diluted with CH_2Cl_2, washed with water, saturated aqueous $NaHCO_3$, saturated aqueous NaCl, dried (Na_2SO_4) and evaporated in vacuo. The resulting solids were purified by flash column chromatography (7:3 dichloromethane/hexanes) to give **18** as a light yellow solid (0.753 g, 92%): mp 75−77 °C; ^{1}H NMR (500 MHz, $CDCl_3$) δ 8.05 (d, J = 9.2 Hz, 1H), 7.61 (d, J = 9.2 Hz, 1H), 3.12−3.05 (m, 4H), 1.49 (t, J = 7.4 Hz, 3H), 1.42 (t, J = 7.5 Hz, 3H); ^{13}C NMR (125 MHz, $CDCl_3$) δ 159.4, 159.2, 146.8, 140.3, 139.2, 129.4, 122.4, 118.7 (q, J_{cf} = 320 Hz), 118.0, 28.2, 28.0, 11.8, 11.5; IR (ATR) cm^{-1} 1596, 1422, 1206; HRMS (ESI-TOF) m/z [M + H]$^+$ Calcd for $C_{13}H_{13}F_3BrN_2O_3S$ 412.9777; Found 412.9778.

*2,3-Diethyl-5,6-bis(phenylethynyl)quinoxaline (**6**).* To an argon degassed solution of **18** (0.753 g, 1.82 mmol) in 1:1 THF/Et_3N (22 mL) was added copper iodide (0.015 g, 0.079 mmol), phenylacetylene (0.569 g, 5.57 mmol) and tetrakis (triphenylphosphine)palladium(0) (0.089 g, 0.077 mmol) and the resulting solution was stirred under argon in the dark for 20 h at 50 °C. GC−MS analysis of the crude reaction mixture indicated a significant amount of monocoupled product remained so an additional portion of phenylacetylene (0.186 g, 1.82 mmol) and tetrakis (triphenylphosphine)palladium(0) (0.045 g, 0.039 mmol) were added and the solution was heated at 50 °C an additional 16 h. Upon completion as judged by TLC, the reaction mixture was diluted with CH_2Cl_2, washed with saturated aqueous NH_4Cl, saturated aqueous NaCl, dried (Na_2SO_4) and evaporated in vacuo. The resulting solids were purified by flash column chromatography (3:1 chloroform/hexanes) to give **6** as a yellow solid (0.297 g, 42%): mp 169−171 °C; ^{1}H NMR (500 MHz, $CDCl_3$) δ 7.92 (d, J = 8.7 Hz, 1H), 7.78 (d, J = 8.6 Hz, 1H), 7.72−7.70 (m, 2H), 7.66−7.64 (m, 2H), 7.40−7.37 (m, 6H), 3.12 (q, J = 7.3 Hz, 2H), 3.06 (q, J = 7.5 Hz, 2H), 1.56 (t, J = 7.3 Hz, 3H), 1.42 (t, J = 7.5 Hz, 3H); ^{13}C NMR (125 MHz, $CDCl_3$) δ 157.9, 141.3, 140.4, 131.9, 131.8, 131.3, 128.7, 128.54, 128.47, 128.4, 126.5, 125.4, 123.8, 123.2, 100.3, 95.8, 88.8, 86.2, 28.3, 28.2, 12.2, 11.4; IR (ATR) cm^{-1} 2204, 1595, 1495, 1453; UV−vis (CH_2Cl_2) λ_{max} (nm) (log ε) 282 (4.70), 289 (4.73), 364 (4.37); Em (CH_2Cl_2; excitation 350 nm) λ_{max} (nm) 429; HRMS (ESI-TOF) m/z [M + H]$^+$ Calcd for $C_{28}H_{23}N_2$ 387.1856; Found 387.1857.

*Benzo[f]quinoxaline (**21**).* A solution of **2** (0.010 g, 0.056 mmol) in chlorobenzene (16 mL) and 1,4-cyclohexadiene (1.3 g, 16 mmol) was placed in an Ace pressure tube and sealed. The reaction was heated to 180 °C in an oil bath for 2 h. After cooling to room temperature the solution was evaporated in vacuo and the resulting solids were purified by flash column chromatography (3:2 hexanes/ethyl acetate) to give **21** as a tan solid (0.0084 g, 84%): mp 56−57 °C (lit[57] 55−57 °C); ^{1}H NMR (500 MHz, $CDCl_3$) δ 9.25−9.23 (m, 1H), 8.94 (d, J = 2.0 Hz, 1H), 8.92 (d, J = 2.0 Hz, 1H), 8.07 (d, J = 9.1 Hz, 1H), 7.98−7.96 (m, 2H), 7.81−7.75 (m, 2H); ^{13}C NMR (125 MHz, $CDCl_3$) δ 144.4, 143.2, 142.8, 141.8, 133.3, 131.8, 131.0, 129.0, 128.0, 127.7, 126.8,

DOI: 10.1021/acs.joc.7b02420
J. Org. Chem. 2017, 82, 13297−13312

124.5; IR (ATR) cm^{-1} 1602, 1492, 1443; HRMS (ESI-FTICR) m/z $[M + H]^+$ Calcd for $C_{12}H_9N_2$ 181.0760; Found 181.0760.

8,9-Diphenylbenzo[f]quinoxaline (22). To an argon degassed solution of **4** (0.050 g, 0.151 mmol) in isopropanol (150 mL) in a quartz reaction vessel was added 1,4-cyclohexadiene (2.40 g, 30.0 mmol) and the vessel was sealed with a septum. The solution was then irradiated in a Rayonet Photochemical Reactor with 16 3000 Å lamps for 4 h. The solution was then evaporated in vacuo and purified by flash column chromatography (4:1 chloroform/hexanes) to give unreacted **4** (0.016 g, 32%) and **22** as a yellow solid (4.3 mg, 13%): mp 197−198 °C; ^{1}H NMR (500 MHz, CD_2Cl_2) δ 9.34 (s, 1H), 9.19 (s, 1H), 8.96 (d, J = 2.0 Hz, 1H), 8.32 (s, 2H), 8.13 (s, 1H), δ 7.37−7.35 (m, 10H); ^{13}C NMR (125 MHz, $CDCl_3$) δ 144.5, 143.3, 143.0, 142.0, 141.8, 141.1, 141.0, 140.7, 132.5, 131.5, 130.2, 130.04, 130.00, 129.8, 128.1, 128.0, 127.2, 127.0, 126.8, 126.4; IR (ATR) cm^{-1} 1597, 1485, 1445; HRMS (ESI-TOF) m/z $[M + H]^+$ Calcd for $C_{24}H_{17}N_2$ 333.1386; Found 333.1384.

2,3-Diethyl-8,9-diphenylbenzo[f]quinoxaline (23). To an argon degassed solution of **6** (0.051 g, 0.132 mmol) in isopropanol (150 mL) in a quartz reaction vessel was added 1,4-cyclohexadiene (2.40 g, 30.0 mmol) and the vessel was sealed with a septum. The solution was then irradiated in a Rayonet Photochemical Reactor with 16 3000 Å lamps for 4 h. The solution was then evaporated in vacuo and purified by flash column chromatography (4:1 chloroform/hexanes) to give unreacted **6** (0.026 g, 51%) and **23** as a yellow solid (4.2 mg, 17%): mp 140−142 °C; ^{1}H NMR (500 MHz, $CDCl_3$) δ 9.28 (s, 1H), 8.00 (d, J = 9.0 Hz, 1H), 7.97 (s, 1H), 7.93 (d, J = 9.0 Hz, 1H), 7.34−7.27 (m, 10H), 3.13 (q, J = 7.5 Hz, 2H), 3.10 (q, J = 7.6 Hz, 2H), 1.49 (t, J = 7.5 Hz, 3H), 1.45 (t, J = 7.6 Hz, 3H); ^{13}C NMR (125 MHz, $CDCl_3$) δ 156.6, 155.5, 141.6, 141.3, 140.9, 140.3, 140.0, 138.9, 132.2, 130.22, 130.18, 130.0, 129.7, 129.6, 127.94, 127.92, 127.0, 126.7, 126.6, 126.0, 28.2, 28.1, 12.9, 12.6; IR (ATR) cm^{-1} 1599, 1485, 1441; HRMS (ESI-FTICR) m/z $[M + H]^+$ Calcd for $C_{28}H_{25}N_2$ 389.2012; Found 389.2011.

(E/Z) 7-Phenyl-6-(phenylmethylene)-6H-cyclopenta[g]-quinoxaline (24-E and 24-Z). To an argon degassed solution of **3** (0.050 g, 0.151 mmol) in isopropanol (150 mL) in a quartz reaction vessel was added 1,4-cyclohexadiene (2.58 g, 32.2 mmol) and the vessel was sealed with a septum. The solution was then irradiated in a Rayonet Photochemical Reactor with 16 3000 Å lamps for 4 h. The solution was then evaporated in vacuo and purified by flash column chromatography (98:2 chloroform/ethyl acetate) to give unreacted **3** (9.2 mg, 18%) and a 2:1 mixture of **24-*E*/*Z*** as a yellow oil (7.5 mg, 18%). The initial fractions of the separation were further purified by flash chromatography (chloroform to 99:1 chloroform/ethyl acetate) to give a pure sample of major product **24-*E***: ^{1}H NMR (500 MHz, $CDCl_3$) δ 8.74 (d, J = 1.9 Hz, 1H), 8.67 (d, J = 1.9 Hz, 1H), 8.20 (s, 1H), 7.88 (s, 1H), 7.61−7.57 (m, 4H), 7.52−7.48 (m, 4H), 7.47−7.44 (m, 2H), 7.43 (s,1H), 7.11 (s, 1H); ^{13}C NMR (125 MHz, $CDCl_3$) δ 149.9, 145.3, 144.3, 144.0, 143.2, 142.4, 138.5, 138.1, 136.2, 135.2, 135.0, 129.5, 129.2, 129.1, 128.9, 128.8, 128.6, 128.2, 123.5, 118.9; HRMS (ESI-FTICR) m/z $[M + H]^+$ Calcd for $C_{24}H_{17}N_2$ 333.1386; Found 333.1385. The last fractions of the separation gave an enriched sample of minor product **24-*Z***: ^{1}H NMR (500 MHz, $CDCl_3$) δ 8.79 (d, J = 1.9 Hz, 1H), 8.77 (d, J = 1.9 Hz, 1H), 8.35 (s, 1H), 7.96 (s, 1H), 7.92 (s, 1H), 7.19 (d, J = 1.1 Hz, 1H), 7.15−7.11 (m, 3H), 7.09−7.05 (m, 5H), 7.01−6.98 (m, 2H); HRMS (ESI-FTICR) m/z $[M + H]^+$ Calcd for $C_{24}H_{17}N_2$ 333.1386; Found 333.1385.

■ ASSOCIATED CONTENT

Supporting Information

The Supporting Information is available free of charge on the ACS Publications website at DOI: 10.1021/acs.joc.7b02420.

Computational details (Tables S1−S10, Figures S1−S4); ^{1}H and ^{13}C NMR spectra of compounds **2**−**6**, **8**, **11**, **13**, **16**−**18**, **21**−**24**; electronic absorbance and emission spectra of compounds **1**−**6**; kinetic plots for cyclization of **1** and **2** (Figures S5−S7) and Cartesian coordinates for geometry-optimized structures (PDF)

■ AUTHOR INFORMATION

Corresponding Authors

*E-mail: ghermanb@csus.edu.

*E-mail: jspence@csus.edu.

ORCID

John D. Spence: 0000-0002-9387-8503

Notes

The authors declare no competing financial interest.

■ ACKNOWLEDGMENTS

Funding for the project has been provided by the Donors of the American Chemical Society Petroleum Research Fund (Grant 55293-UR4); the California State University Program in Education and Research in Biotechnology (CSUPERB); the California State University, Sacramento, Research and Creative Activity (RCA) grant, Instructionally Related Activities (IRA) grants and Academically Related Activities (ARA) grants.

■ REFERENCES

(1) Mohamed, R. K.; Peterson, P. W.; Alabugin, I. V. *Chem. Rev.* **2013**, *113*, 7089.

(2) (a) Jones, R. R.; Bergman, R. G. *J. Am. Chem. Soc.* **1972**, *94*, 660. (b) Bergman, R. G. *Acc. Chem. Res.* **1973**, *6*, 25.

(3) (a) Prall, M.; Wittkopp, A.; Schreiner, P. R. *J. Phys. Chem. A* **2001**, *105*, 9265. (b) Vavilala, C.; Byrne, N.; Kraml, C. M.; Ho, D. M.; Pascal, R. A. *J. Am. Chem. Soc.* **2008**, *130*, 13549.

(4) (a) Myers, A. G.; Kuo, E. Y.; Finney, N. S. *J. Am. Chem. Soc.* **1989**, *111*, 8057. (b) Nagata, R.; Yamanaka, H.; Okazaki, E.; Saito, I. *Tetrahedron Lett.* **1989**, *30*, 4995.

(5) Schmittel, M.; Strittmatter, M.; Kiau, S. *Tetrahedron Lett.* **1995**, *36*, 4975.

(6) (a) Galm, U.; Hager, M. H.; Van Lanen, S. G.; Ju, J.; Thorson, J. S.; Shen, B. *Chem. Rev.* **2005**, *105*, 739. (b) *Enediyne Antibiotics as Antitumor Agents*; Borders, D. B., Doyle, T. W., Eds.; Marcel Dekker: New York, 1995. (c) *Neocarzinostatin: The Past, Present, and Future of an Anticancer Drug*; Maeda, H., Edo, K., Ishida, N., Eds.; Springer: New York, 1997.

(7) (a) Nicolaou, K. C.; Dai, W.-M. *Angew. Chem., Int. Ed. Engl.* **1991**, *30*, 1387. (b) Maier, M. E. *Synlett* **1995**, *1995*, 13. (c) Grissom, J. W.; Gunawardena, G. U.; Klingberg, D.; Huang, D. *Tetrahedron* **1996**, *52*, 6453. (d) Kar, M.; Basak, A. *Chem. Rev.* **2007**, *107*, 2861.

(8) (a) Bowles, D. M.; Palmer, G. J.; Landis, C. A.; Scott, J. L.; Anthony, J. E. *Tetrahedron* **2001**, *57*, 3753. (b) Raviola, C.; Protti, S.; Ravelli, D.; Fagnoni, M. *Chem. Soc. Rev.* **2016**, *45*, 4364.

(9) (a) John, J. A.; Tour, J. M. *J. Am. Chem. Soc.* **1994**, *116*, 5011. (b) Rule, J. D.; Moore, J. S. *Macromolecules* **2005**, *38*, 7266. (c) Xiao, Y.; Hu, A. *Macromol. Rapid Commun.* **2011**, *32*, 1688.

(10) Sun, Q.; Zhang, C.; Li, Z.; Kong, H.; Tan, Q.; Hu, A.; Xu, W. *J. Am. Chem. Soc.* **2013**, *135*, 8448.

(11) Halter, R. J.; Fimmen, R. L.; McMahon, R. J.; Peebles, S. A.; Kuczkowski, R. L.; Stanton, J. F. *J. Am. Chem. Soc.* **2001**, *123*, 12353.

(12) (a) Schreiner, P. R.; Navarro-Vazquez, A.; Prall, M. *Acc. Chem. Res.* **2005**, *38*, 29. (b) Sherer, E. C.; Kirschner, K. N.; Pickard, F. C., IV; Rein, C.; Feldgus, S.; Shields, G. C. *J. Phys. Chem. B* **2008**, *112*, 16917. (c) Kraka, E.; Cremer, D. *WIREs Comput. Mol. Sci.* **2014**, *4*, 285.

(13) (a) Stahl, F.; Moran, D.; Schleyer, P. v. R.; Prall, M.; Schreiner, P. R. *J. Org. Chem.* **2002**, *67*, 1453. (b) De Proft, F.; Schleyer, P. v. R.; Lenthe, J. H. v.; Stahl, F.; Geerlings, P. *Chem. - Eur. J.* **2002**, *8*, 3402.

(14) (a) Roth, W. R.; Hopf, H.; Horn, C. *Chem. Ber.* **1994**, *127*, 1765. (b) Roth, W. R.; Hopf, H.; Wasser, T.; Zimmermann, H.; Werner, C. *Liebigs Annal.* **1996**, *1996*, 1691. (c) Prall, M.; Wittkopp, A.; Schreiner, P. R. *J. Phys. Chem. A* **2001**, *105*, 9265.

(15) Koseki, S.; Fujimura, Y.; Hirama, M. *J. Phys. Chem. A* **1999**, *103*, 7672.
(16) Kaneko, T.; Takahashi, M.; Hirama, M. *Tetrahedron Lett.* **1999**, *40*, 2015.
(17) Lockhart, T. P.; Comita, P. B.; Bergman, R. G. *J. Am. Chem. Soc.* **1981**, *103*, 4082.
(18) Choy, N.; Kim, C. S.; Ballestero, C.; Artigas, L.; Diez, C.; Lichtenberg, F.; Shapiro, J.; Russell, K. C. *Tetrahedron Lett.* **2000**, *41*, 6955.
(19) (a) Galbraith, J. M.; Schreiner, P. R.; Harris, N.; Wei, W.; Wittkopp, A.; Shaik, S. *Chem. - Eur. J.* **2000**, *6*, 1446. (b) Alabugin, I. V.; Manoharan, M. *J. Phys. Chem. A* **2003**, *107*, 3363.
(20) (a) Alabugin, I. V.; Manoharan, M.; Kovalenko, S. V. *Org. Lett.* **2002**, *4*, 1119. (b) Zeidan, T. A.; Manoharan, M.; Alabugin, I. V. *J. Org. Chem.* **2006**, *71*, 954. (c) Zeidan, T. A.; Kovalenko, S. V.; Manoharan, M.; Alabugin, I. V. *J. Org. Chem.* **2006**, *71*, 962. (d) Pickard, F. C., IV; Shepherd, R. L.; Gillis, A. E.; Dunn, M. E.; Feldgus, S.; Kirschner, K. N.; Shields, G. C.; Manoharan, M.; Alabugin, I. V. *J. Phys. Chem. A* **2006**, *110*, 2517.
(21) (a) Alabugin, I. V.; Manoharan, M. *J. Am. Chem. Soc.* **2003**, *125*, 4495. (b) Peterson, P. W.; Shevchenko, N.; Breiner, B.; Manoharan, M.; Lufti, F.; Delaune, J.; Kingsley, M.; Kovnir, K.; Alabugin, I. V. *J. Am. Chem. Soc.* **2016**, *138*, 15617.
(22) Schmittel, M.; Kiau, S. *Chem. Lett.* **1995**, *24*, 953.
(23) Korovina, N. V.; Chang, M. L.; Nguyen, T. T.; Fernandez, R.; Walker, H. J.; Olmstead, M. M.; Gherman, B. F.; Spence, J. D. *Org. Lett.* **2011**, *13*, 3660.
(24) Lewis, K. D.; Matzger, A. J. *J. Am. Chem. Soc.* **2005**, *127*, 9968.
(25) Spence, J. D.; Rios, A. C.; Frost, M. A.; McCutcheon, C. M.; Cox, C. D.; Chavez, S.; Fernandez, R.; Gherman, B. F. *J. Org. Chem.* **2012**, *77*, 10329.
(26) (a) Jones, G. B.; Russell, K. C. The Photo-Bergman Cycloaromatization of Enediynes. In *CRC Handbook of Organic Photochemistry and Photobiology*, 2nd ed.; Horspool, W., Lenci, F., Eds.; CRC Press: Boca Raton, FL, 2004; pp 29−1. (b) Alabugin, I. V.; Yang, W.-Y.; Pal, R. Photochemical Bergman Cyclization and Related Photoreactions of Enediynes. In *CRC Handbook of Organic Photochemistry and Photobiology*, 3rd ed.; Griesbeck, A., Oelgemoller, M., Ghetti, F., Eds.; CRC Press: Boca Raton, FL, 2012; Vol. *1*, pp 549−592.
(27) (a) Turro, N. J.; Evenzahav, A.; Nicolaou, K. C. *Tetrahedron Lett.* **1994**, *35*, 8089. (b) Evenzahav, A.; Turro, N. J. *J. Am. Chem. Soc.* **1998**, *120*, 1835.
(28) Funk, R. L.; Young, E. R. R.; Williams, R. M.; Flanagan, M. F.; Cecil, T. L. *J. Am. Chem. Soc.* **1996**, *118*, 3291.
(29) Jones, G. B.; Wright, J. M.; Plourde, G., II; Purohit, A. D.; Wyatt, J. K.; Hynd, G.; Fouad, F. *J. Am. Chem. Soc.* **2000**, *122*, 9872.
(30) Kaneko, T.; Takanashi, M.; Hirama, M. *Angew. Chem., Int. Ed.* **1999**, *38*, 1267.
(31) Spence, J. D.; Hargrove, A. E.; Crampton, H. L.; Thomas, D. W. *Tetrahedron Lett.* **2007**, *48*, 725.
(32) Kovalenko, S. V.; Peabody, S.; Manoharan, M.; Clark, R. J.; Alabugin, I. V. *Org. Lett.* **2004**, *6*, 2457.
(33) (a) Pangamte, H. N.; Lyngdoh, R. H. D. *J. Phys. Chem. A* **2010**, *114*, 2710. (b) Dong, H.; Chen, B. Z.; Huang, M. B.; Lindh, R. *J. Comput. Chem.* **2012**, *33*, 537.
(34) (a) Hoffmann, R.; Imamura, A.; Hehre, W. J. *J. Am. Chem. Soc.* **1968**, *90*, 1499. (b) Hoffmann, R. *Acc. Chem. Res.* **1971**, *4*, 1.
(35) Squires, R. R.; Cramer, C. J. *J. Phys. Chem. A* **1998**, *102*, 9072.
(36) Alabugin, I. V.; Manoharan, M. *J. Am. Chem. Soc.* **2003**, *125*, 4495.
(37) Peterson, P. W.; Mohamed, R. K.; Alabugin, I. V. *Eur. J. Org. Chem.* **2013**, *2013*, 2505.
(38) (a) Sonogashira, K.; Tohda, Y.; Hagihara, N. *Tetrahedron Lett.* **1975**, *16*, 4467. (b) Chinchilla, R.; Najera, C. *Chem. Rev.* **2007**, *107*, 874.
(39) Wasik, R.; Winska, P.; Poznanski, J.; Shugar, D. *J. Phys. Chem. B* **2012**, *116*, 7259.
(40) Minisci, F.; Vismara, E.; Fontana, F. *Heterocycles* **1989**, *28*, 489.
(41) (a) Grissom, J. W.; Calkins, T. L. *J. Org. Chem.* **1993**, *58*, 5422. (b) Grissom, J. W.; Calkins, T. L.; McMillen, H. A.; Jiang, Y. H. *J. Org. Chem.* **1994**, *59*, 5833. (c) Grissom, J. W.; Gunawardena, G. U. *Tetrahedron Lett.* **1995**, *36*, 4951.
(42) Zeidan, T. A.; Kovalenko, S. V.; Manoharan, M.; Alabugin, I. V. *J. Org. Chem.* **2006**, *71*, 962.
(43) At the highest 1,4-cyclohexadiene concentration studied, **20** contributes approximately 15% of the total product mixture through first reaction half-life.
(44) Data points at the lowest 1,4-cyclohexadiene concentration, where polymerization of the diradical intermediate likely occurs, were not included in plots.
(45) Vinogradova, O. V.; Balova, I. A.; Popik, V. V. *J. Org. Chem.* **2011**, *76*, 6937.
(46) Zhao, Z.; Peng, Y.; Dalley, N. K.; Cannon, J. F.; Peterson, M. A. *Tetrahedron Lett.* **2004**, *45*, 3621.
(47) (a) Schmittel, M.; Strittmatter, M.; Kiau, S. *Tetrahedron Lett.* **1995**, *36*, 4975. (b) Schmittel, M.; Keller, M.; Kiau, S.; Strittmatter, M. *Chem. - Eur. J.* **1997**, *3*, 807.
(48) For a discussion on C^1-C^5 versus C^1-C^6 cyclization of enediynes under thermal conditions, see: (a) Lewis, K. D.; Matzger, A. J. *J. Am. Chem. Soc.* **2005**, *127*, 9968. (b) Vavilala, C.; Byrne, N.; Kraml, C. M.; Ho, D. M.; Pascal, R. A. *J. Am. Chem. Soc.* **2008**, *130*, 13549.
(49) For additional examples of radical promoted C^1-C^5 cyclization of enediynes, see: Peabody, S. W.; Breiner, B.; Kovalenko, S. V.; Patil, S.; Alabugin, I. V. *Org. Biomol. Chem.* **2005**, *3*, 218. For related reductive cyclizations, see: (a) Whitlock, H. W.; Sandvick, P. E.; Overman, L. E.; Reichardt, P. B. *J. Org. Chem.* **1969**, *34*, 879. (b) Alabugin, I. V.; Kovalenko, S. V. *J. Am. Chem. Soc.* **2002**, *124*, 9052. (c) Peterson, P. W.; Shevchenko, N.; Breiner, B.; Manoharan, M.; Lufti, F.; Delaune, J.; Kingsley, M.; Kovnir, K.; Alabugin, I. V. *J. Am. Chem. Soc.* **2016**, *138*, 15617.
(50) Frisch, M. J.; Trucks, G. W.; Schlegel, H. B.; Scuseria, G. E.; Robb, M. A.; Cheeseman, J. R.; Scalmani, G.; Barone, V.; Mennucci, B.; Petersson, G. A.; Nakatsuji, H.; Caricato, M.; Li, X.; Hratchian, H. P.; Izmaylov, A. F.; Bloino, J.; Zheng, G.; Sonnenberg, J. L.; Hada, M.; Ehara, M.; Toyota, K.; Fukuda, R.; Hasegawa, J.; Ishida, M.; Nakajima, T.; Honda, Y.; Kitao, O.; Nakai, H.; Vreven, T.; Montgomery, J. A., Jr.; Peralta, J. E.; Ogliaro, F.; Bearpark, M.; Heyd, J. J.; Brothers, E.; Kudin, K. N.; Staroverov, V. N.; Keith, T.; Kobayashi, R.; Normand, J.; Raghavachari, K.; Rendell, A.; Burant, J. C.; Iyengar, S. S.; Tomasi, J.; Cossi, M.; Rega, N.; Millam, J. M.; Klene, M.; Knox, J. E.; Cross, J. B.; Bakken, V.; Adamo, C.; Jaramillo, J.; Gomperts, R.; Stratmann, R. E.; Yazyev, O.; Austin, A. J.; Cammi, R.; Pomelli, C.; Ochterski, J. W.; Martin, R. L.; Morokuma, K.; Zakrzewski, V. G.; Voth, G. A.; Salvador, P.; Dannenberg, J. J.; Dapprich, S.; Daniels, A. D.; Farkas, O.; Foresman, J. B.; Ortiz, J. V.; Cioslowski, J.; Fox, D. J. *Gaussian 09*, Revision C.01; Gaussian, Inc.: Wallingford, CT, 2010.
(51) Adamo, C.; Barone, V. *J. Chem. Phys.* **1998**, *108*, 664.
(52) Perdew, J. P.; Chevary, J. A.; Vosko, S. H.; Jackson, K. A.; Pederson, M. R.; Singh, D. J.; Fiolhais, C. *Phys. Rev. B: Condens. Matter Mater. Phys.* **1992**, *46*, 6671.
(53) Chen, Z.; Wannere, C. S.; Corminboeuf, C.; Puchta, R.; Schleyer, P. v. R. *Chem. Rev.* **2005**, *105*, 3842.
(54) (a) Schleyer, P. v. R.; Jiao, H.; Hommes, N. J. R. v. E.; Malkin, V. G.; Malkina, O. L. *J. Am. Chem. Soc.* **1997**, *119*, 12669. (b) Schleyer, P. v. R.; Manoharan, M.; Wang, Z.-X.; Jiao, H.; Puchta, R.; Hommes, N. J. R. v. E. *Org. Lett.* **2001**, *3*, 2465.
(55) Cramer, C. J. *Essentials of Computational Chemistry: Theories and Models*, 2nd ed.; John Wiley & Sons, Ltd.: West Sussex, England, 2004.
(56) Wiitala, K. W.; Hoye, T. R.; Cramer, C. J. *J. Chem. Theory Comput.* **2006**, *2*, 1085−1092.
(57) Chung, T. F.; Wu, Y. M.; Cheng, C. H. *J. Org. Chem.* **1984**, *49*, 1215.

DOI: 10.1021/acs.joc.7b02420
J. Org. Chem. 2017, 82, 13297−13312